



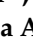



Review

Heterogeneous Catalysts for Conversion of Biodiesel-Waste Glycerol into High-Added-Value Chemicals

Nabila Tabassum ^{1,†}, Ramyakrishna Pothu ^{2,†}, Aishanee Pattnaik ³, Rajender Boddula ^{3,*}, Putrakumar Balla ³, Raveendra Gundeboyina ³, Prathap Challa ³, Rajendiran Rajesh ³, Vijayanand Perugopu ^{3,*}, Naresh Mamede ⁴, Ahmed Bahgat Radwan ⁵, Aboubakr M. Abdullah ⁵ and Noora Al-Qahtani ^{5,*}

- ¹ Department of Chemical Engineering, Shiv Nadar University, Greater Noida 201314, Uttar Pradesh, India; naveelatabassum999@gmail.com
- ² School of Physics and Electronics, College of Chemistry and Chemical Engineering, Hunan University, Changsha 410082, China; research.ramyakrishna@gmail.com
- ³ Energy & Environmental Engineering Department, CSIR—Indian Institute of Chemical Technology, Hyderabad 500007, Telangana State, India; pattnaik.aishanee@gmail.com (A.P.); bputrakumar@yahoo.com (P.B.); graveendra905@gmail.com (R.G.); prathap.challa@gmail.com (P.C.); rrajchem7@gmail.com (R.R.)
- ⁴ Department of Engineering Chemistry, College of Engineering, Koneru Lakshmaiah Education Foundation, Vaddeswaram 522303, Andhra Pradesh, India; mamedanaresh@gmail.com
- ⁵ Center for Advanced Materials (CAM), Qatar University, Doha 2713, Qatar; ahmedbahgat@qu.edu.qa (A.B.R.); bakr@qu.edu.qa (A.M.A.)
- * Correspondence: research.raaj@gmail.com (R.B.); pvanand@iict.res.in (V.P.); noora.alqahtani@qu.edu.qa (N.A.-Q.)
- † These authors equally contributed to this work.



Citation: Tabassum, N.; Pothu, R.; Pattnaik, A.; Boddula, R.; Balla, P.; Gundeboyina, R.; Challa, P.; Rajesh, R.; Perugopu, V.; Mamede, N.; et al. Heterogeneous Catalysts for Conversion of Biodiesel-Waste Glycerol into High-Added-Value Chemicals. *Catalysts* **2022**, *12*, 767. <https://doi.org/10.3390/catal12070767>

Academic Editors: Karine De Oliveira Vigier and Binlin Dou

Received: 24 May 2022

Accepted: 4 July 2022

Published: 11 July 2022

Publisher's Note: MDPI stays neutral with regard to jurisdictional claims in published maps and institutional affiliations.



Copyright: © 2022 by the authors. Licensee MDPI, Basel, Switzerland. This article is an open access article distributed under the terms and conditions of the Creative Commons Attribution (CC BY) license (<https://creativecommons.org/licenses/by/4.0/>).

Abstract: The valuable products produced from glycerol transformation have become a research route that attracted considerable benefits owing to their huge volumes in recent decades (as a result of biodiesel production as a byproduct) as well as a myriad of chemical and biological techniques for transforming glycerol into high-value compounds, such as fuel additives, biofuels, precursors and other useful chemicals, etc. Biodiesel has presented another challenge in the considerable increase in its byproduct (glycerol). This review provides a recent update on the transformation of glycerol with an exclusive focus on the various catalysts' performance in designing reaction operation conditions. The different products observed and cataloged in this review involved hydrogen, acetol, acrolein, ethylene glycol, and propylene glycol (1,3-propanediol and 1,2-propanediol) from reforming and dehydration and hydrogenolysis reactions of glycerol conversions. The future prospects and critical challenges are finally presented.

Keywords: glycerol; biodiesel-biowaste; value-added products; hydrogen energy; lignocellulosic biomass valorization; fuels; catalysts

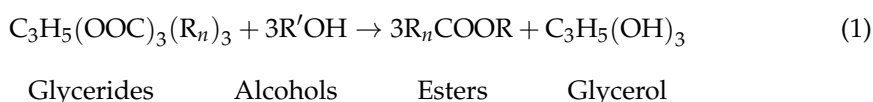
1. Introduction

Petroleum fuels became the primary energy source for transport requirements during the twentieth century. Since the beginning of the twenty-first century, primarily all vehicles run with diesel, gasoline, or natural gas [1]. Around the world, the population is increasing, thereby increasing energy requirements simultaneously, and nowadays, the origin of energy is mostly fossil fuels such as oil, coal, or natural gas [2–4]. Generally, fossil fuel-based carbon dioxide emissions are unaltered and grant the so-called “greenhouse effect”, which intensively affects the climate changes [5,6]. Furthermore, with the rise in pollution and crude oil prices, oil, coal, and gas burn not only to fulfill energy demands, but also contribute to the global warming crisis. The burning of fossil fuels produces a substantial amount of carbon dioxide, which traps heat in the atmosphere and contributes to global

warming [7,8]. Wind, water, biomass, and solar energy are primary alternative energy sources to stop using fossil fuels.

Biomass is currently achieving a significant focus in terms of providing the world's energy needs [9–11]. Due to its eco-friendly nature and low sulfur production, it is estimated that by 2050, biomass will contribute 50% of the total energy demand. The demand for energy worldwide is expected to increase up to 48% by 2040 [10]. Thus, bio-derived fossil fuels are crucial for reducing the carbon footprint [9–11].

Biodiesel is commonly manufactured from animal fat or vegetable oil, and through the transesterification technique, glycerol is produced as a waste product (Equation (1)) [12]. Biodiesel production is growing continuously due to the growing fossil fuel demand for transportation and industries. The biodiesel trend enhanced glycerol production as a byproduct [11]. Glycerol contains higher hydrogen moles compared to ethanol and methanol [13]. Each 1 ton of biodiesel production from plants produces 110 kg of glycerol. Worldwide glycerol production was increased five-fold to reach 36 billion liters between 2006–2018 [14]. It is pretty clear that glycerol availability is not in doubt; it is believed that generally, glycerol production will continue to increase due to an upsurge in biodiesel production. Glycerol was raised as an exciting biomass feedstock for high-value-added product conversion due to its modest price and high availability in the market [15]. Hence, glycerol transformation into other useful products is the essence of overall improvement in biodiesel production economics [16].



Glycerol is crucial for feedstocks in food, pharmaceutical, and other industries and is produced through microbial or biodiesel. Semkiv et al. explained glycerol production by microbes (*Saccharomyces cerevisiae*, Osmotolerant yeasts, Microalgae, and cyanobacteria). High-added value chemicals produced from glycerol follow different paths such as oxidation, reforming, carbonylation, acetalization, esterification, hydrogenolysis, dehydration, etc., as shown in Table 1 [16–21]. Glycerol-based additives have been used for blending agents in gasoline, diesel fuel, and biodiesel [22].

Table 1. Derivatives of glycerol.

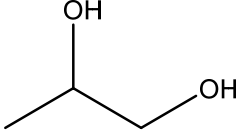
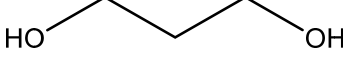
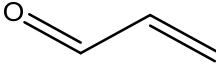

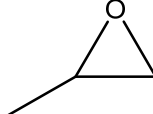
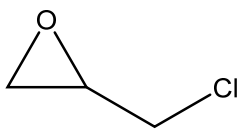
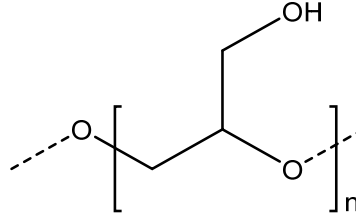
Chemical Derivative	Chemical Structure	Route from Glycerol
Syngas	H ₂ + CO	Reforming
1,2 Propanediol		hydrogenolysis
1,3 Propanediol		hydrogenolysis
Acrolein		Dehydration
Ethylene oxide		Via 1,2 propanediol
Propylene oxide		Via 1,3 propanediol

Table 1. Cont.

Chemical Derivative	Chemical Structure	Route from Glycerol
Epichlorohydrin		Cyclization
Polyglycerol		Oligomerization

Martin and Richter presented a review for glycerol oligomerization to diglycerol and triglycerol, focusing on utilizing acidic and basic heterogeneous catalysts. Pure glycerol was replaced through its oligomers for numerous uses in the cosmetics and food industries [23]. Razali and Abdullah presented a review for catalyzing glycerol to lactic acid, where mixed metal oxides and bimetallic catalysts were found to be promising candidates [24]. Most of the published reviews have summarized the chemo, as well as biocatalytic transesterification and economic aspects of various transformation routes discussed [25,26]. A few comprehensive reviews have been published on the catalytic conversion of glycerol via reforming, dehydration, and hydrogenolysis. Since glycerol transformation is rapidly developing and its critical features are not clear, it is important to gather information on recent developments. Consequently, the objective of this review is to provide an update on the transformation of glycerol derived from biodiesel plants using heterogeneous catalysts into different products (chemicals, fuel additives, fuels). The review is organized well into three sections, dedicated to three major types of reactions (reforming, dehydration, and hydrogenolysis), with an emphasis on the performance of catalysts in designing reaction conditions. The different products observed and cataloged in this review involved hydrogen, acetol, acrolein, ethylene glycol, 1,3-propanediol (1,3-PDO), and 1,2-propanediol (1,2-PDO) from reforming, dehydration and hydrogenolysis reactions of glycerol conversions.

The production of chemical products from the catalytic transformation of glycerol is shown in Figure 1. Glycerol is produced from the transesterification of biodiesel and vegetable oils and animal fats, and the fermentation of carbohydrates. Syngas produced from glycerol yield liquid hydrocarbons, methanol, and other value-added products from the Fischer–Tropsch process. Syngas through the water–gas shift reaction produces liquid hydrocarbons, which include diesel, liquid naphtha, etc. Furthermore, through the methanol synthesis process, syngas produces methanol, and further methanol is used for the transesterification process and to produce chemicals [27].

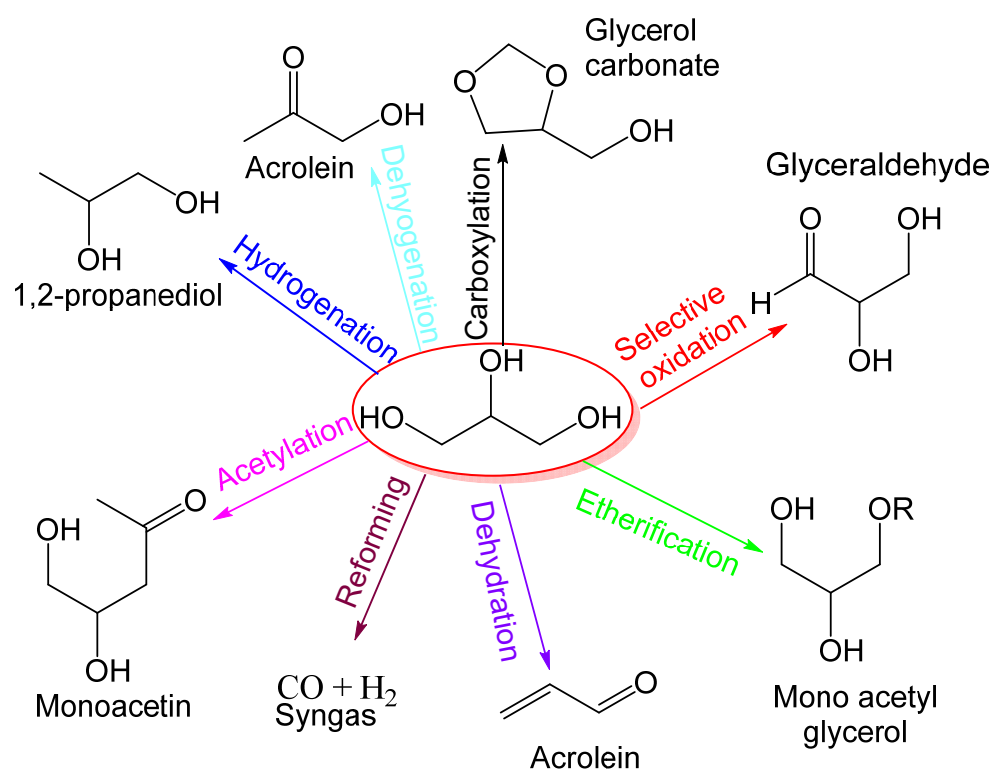


Figure 1. Catalytic transformation of glycerol to various different products.

2. Glycerol Reforming

The glycerol transformation carried out through combustion in the past was unsafe, uneconomic, and technically deficient due to the high temperature employed, unwanted gas emission, and complex product [27,28]. Reforming techniques have gained acceptance by industrialists and researchers in view of their efficiencies. Steam, aqueous, and autothermal reforming processes have been primarily investigated in glycerol reforming. The steam reforming reaction is one of the most common reactions used in hydrogen synthesis. Low pressure and very endothermic reactions promote hydrogen selectivity. The aqueous phase reforming (APR) method is regarded as an inexpensive method for producing H₂ due to its lower temperature and lack of vaporizing water and fuels [29,30]. Glycerol has a wide product distribution due to its complexity compared to low-chain hydrocarbons or alcohols and to the numerous reactions associated with the reforming process (Figure 2). However, this technique creates H₂ without vaporizing the feedstock, resulting in significant energy savings [31]. Supercritical water gasification (SCWG) is a cost-effective method of turning biomass (such as food waste, paper industrial waste, sewage sludge, agricultural waste, and forestry residue) into hydrogen-rich syngas [32]. Chemical looping steam reforming (CLSR), which uses oxygen carriers (OCs) as a catalyst, has been widely recognized as a highly effective method for generating hydrogen from catalytic steam reforming [33].

Bio-derived liquids steam reforming produces hydrogen and becomes interested due to the environment and raises hydrogen demand, specifically in proton-exchange membrane fuel cells (PEMFC) [34]. The low temperature and high-pressure process conditions, concentrated feed, and acidic catalysts are used for the supercritical water reforming process. High temperature and low pressure, diluted feed, and alkali catalyst are used for gasification [35].

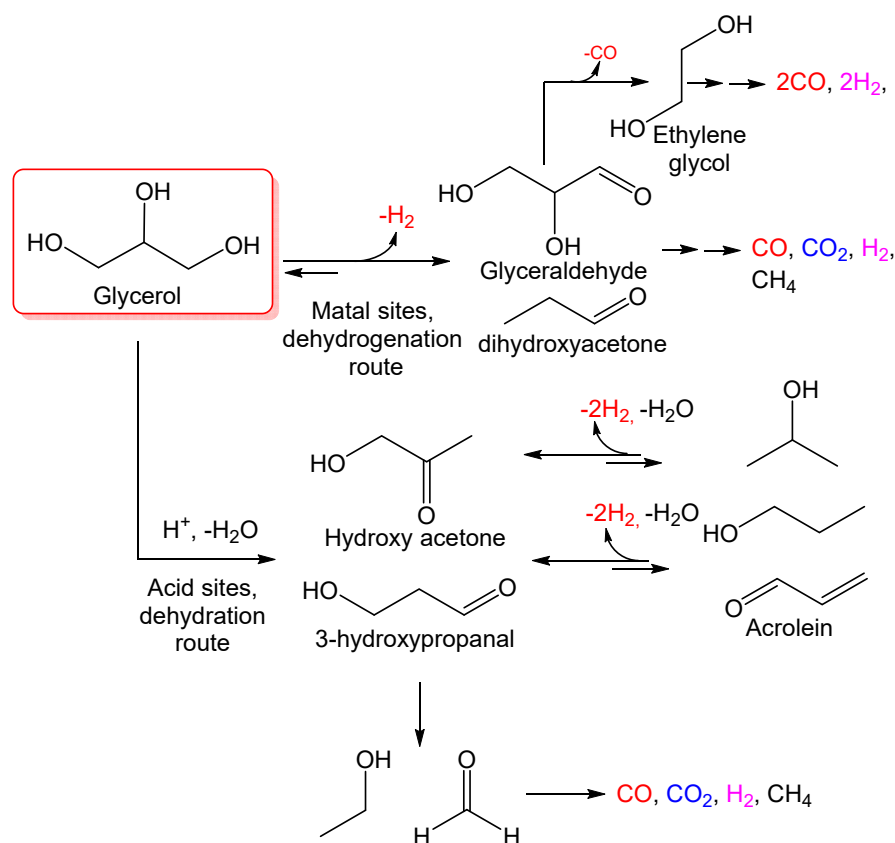


Figure 2. Potential reaction pathways in glycerol aqueous phase reforming (APR).

The glycerol reforming and endothermic reactions took place. Hence, the heat needed for the decomposition of glycerol (Equation (2)) is significantly larger than the water–gas shift (WGS) reaction (Equation (3)), where heat is produced as energy. As operated under atmospheric pressure, glycerol steam reforming (Equation (4)) becomes desirable with less fear of protection. Considerably, 1 mol of glycerol converts to produce 7 mol of hydrogen (Equation (3)). Vast amounts of steam and elevated temperature shift a reaction forward to equilibrium, and hence much more H_2 is generated [36].



The mentioned noble metal catalysts, Pt [37,38], Ir [39], Ru [40], and Rh [41,42], have shown good resistance to coke and catalytic activity. Vaidya and Rodrigues studied Ni, Pt, and Ru catalysts that promote hydrogen production but cause deactivation by dehydration [43].

2.1. Platinum Catalysts for Glycerol Reforming

Doukkali et al. investigated Pt and/or Ni supported over γ -alumina catalyst for the generation of hydrogen by a method of APR through three preparation methods of catalyst: impregnation method, and sol-gel in acidic and basic medium. Total glycerol transformation occurred with maximum hydrogen production by sol-gel in basic method over PtNiAl ($T = 250\text{ }^\circ\text{C}$, $P = 30\text{ bar}$, and $WHSV = 2.6\text{ hr}^{-1}$). The acidity of the superficial hydroxyl groups on the $-AlOOH$ surface could be to blame for the lower glycerol conversion into gaseous products, favoring dehydration processes and resulting in more OHCs in the liquid phase. In fact, by blocking surface hydroxyl sites on $-Al_2O_3$, structural alterations in hydrothermal settings were explored to create efficient alumina catalysts for APR pro-

cesses. The drop in H₂ production could be explained by Ni particle aggregation and reoxidation of Ni particles. These behaviors combined with the adsorption of carbonaceous molecules/organic compounds identified on several of the catalysts could be the primary causes of their deactivation [37].

Pompeo et al. investigated SiO₂ catalyst supported with Pt and Ni through the ion-exchange method for steam reforming to produce hydrogen. The experiment for the steam reforming reaction of glycerol has demonstrated that using 1 Pt and 2 Pt catalysts. The more active and stable catalyst was Pt compared to Ni catalyst. At 350 °C, a complete conversion to gas was achieved with a space-time of 1.66 and 0.88 min, respectively. Due to the fact that the Ni catalyzed the WGS reaction to remove the CO adsorbed on the surface and turn it into CO₂, the selectivity of gas products was significantly different. Only 3% CO was obtained using the 5 Ni catalyst at 450 °C for 1.66 min. During 40 hr activity test on stream at 350 °C, the 2 Pt catalyst allowed entire conversion to gas without deactivation. It was also suggested that bimetallic catalyst research is required to obtain a system with high selectivity for H₂ and good stability [38].

2.2. Ruthenium Catalysts for Glycerol Reforming

Ru catalyst supported over core-shell metal-ceramic micro composites, created at low temperature and 1 atm pressure through microwave-induced hydrothermal oxidation technique (MW-HTO) of aluminum (Al) metal particles. The highest glycerol turnover ratio was achieved over Al, and Ru-modified Al₂O₃ at Al compared with Ru-modified MgAl₂O₄ and Ru-modified Al₂O₃ catalysts, suggesting that Al metal particles seem to be more effective in preparing MgAl₂O₄ at Al and Al₂O₃ at Al composite structure. The highest selectivity of hydrogen was 70% at Ru/MgAl₂O₄ at Al catalyst at 823 K reaction temperature, 1 atm pressure with 870 mmg_{cat}⁻¹ h⁻¹ feed flow rate. The Ru/MgAl₂O₄@Al and Ru/Al₂O₃@Al catalysts have 2–3 times the glycerol conversion rates of their Ru/MgAl₂O₄ and Ru/Al₂O₃ counterparts, owing to enhanced heat transfer via the metal-ceramic composite catalytic architectures [40]. Glycerol steam reforming process over Ru doped Al₂O₃ catalyst. In total, 89.1% glycerol transformed to produce 0.49 (mol/mol) yield of hydrogen at T = 500 °C, P = 0.1 MPa and 1.98 W/FA0. This research has aided in developing reactor systems for producing hydrogen from glycerol steam reforming [41].

2.3. Rhodium Catalysts for Glycerol Reforming

Martinez et al. studied hydrogen production from glycerol reforming using fluorite-type oxides CeZr-CoRh prepared by the sol-gel method. 100% glycerol was transformed to produce 86% hydrogen yield at 650 °C. The activity data showed that the catalysts' ability to activate H₂O under reaction circumstances was connected to selective H₂ generation. This process guarantees that the by-products are steam reformed to H₂. As this capacity deteriorates, H₂ generation decreases, steam reforming capability reduces, and glycerol decomposition takes over. In this scenario, the creation of condensable compounds, such as hydroxyacetone, acetaldehyde, and acrolein, was aided by the production of CO, CH₄, and C₂H₄ [44].

Lee and Doohwan synthesized Core-shell MgAl₂O₄ metal-ceramic composites at Al catalyst by hydrothermal method, and Rh (1, 3, and 5 wt.% loading) modified MeAl₂O₄ catalysts were synthesized by incipient wetness impregnation method. Then, 100% glycerol transformed to produce Rh/MgAl₂O₄ at Al catalyst [T = 450 °C, and WHSV = 34,000 mL g⁻¹ h⁻¹]. The high surface area and complex surface morphological properties of MeAl₂O₄@Al as a catalyst enhance increased Rh cluster dispersion while hindering their thermal sintering during glycerol steam reforming processes at high temperatures. Rh/MeAl₂O₄@Al had a 20–30% greater glycerol conversion turnover rate than Rh/MeAl₂O₄ (both Rh cluster sizes are similar), indicating that the facilitated heat and mass transfer through the unique MeAl₂O₄@Al microstructures cooperated constructively for the reactions. These are being explored as future research topics [45]. Baca et al. studied Rh, Ni, and Co metal-doped over Al₂O₃-ZrO₂-TiO₂ (AZT) for syngas production through carbon dioxide reforming

of glycerol. Then, 1 wt.% Rh doped AZT, 5 wt.% Ni-doped AZT, and 5 wt.% Co-doped AZT catalysts were synthesized through the incipient impregnation method. The glycerol transformation was 80% achieved with 24% maximum hydrogen yield on Rh doped AZT catalyst at 750 °C. Glycerol Conversion reduced in the given sequence: 1% Rh doped AZT > 5% Ni doped AZT > 5% Co-doped AZT. Rh doped AZT catalyst remained stable due to fewer coke formations and a shortage of sintering. During the 72-h testing, the decrease in CO₂ conversions was less than 13%, indicating the remarkable stability of Rh/AZT and Ni/AZT [42]. Delparish et al. produced syngas from glycerol by oxidative steam reforming. The impregnation technique was used to prepare 2 wt.% of Rh doped Al₂O₃ catalysts. The glycerol was completely converted at 550 °C, and maximum hydrogen yield was achieved at 700 °C. Temperature influenced product distribution by increasing the amount of combustible species in the product mixture that were oxidized. The effect became more severe when C/O was lowered from 1.125 to 0.75. The promotion of WGS in the presence of steam was confirmed by reducing S/C from 5 to 4 and then from 4 to 3, which resulted in monotonically decreased H₂ and CO₂ yields and an increase in CO yield [46]. Danga et al. studied glycerol and ethanol for dry reforming with CaCO₃ to produce syngas. A series of metal components, such as nickel, iron, copper, platinum, palladium, ruthenium, and rhodium, were used to promote dry reforming. In these series of metals, nickel became a promising candidate due to its outstanding performance, as well as its low price. Here, 100% glycerol conversion along with approximate 92% syngas selectivity achieved on 10 wt.% Ni contained in CaCO₃ catalyst [T = 550 °C, and P = 1 atm.]. The CO₂ released from the CaCO₃ catalyst eliminated cokes and attained stability. The direct use of CaCO₃ in this process was discovered viable, and the CO₂ generated from CaCO₃ decomposition may be used to modify the H₂/CO ratio. Ni was the most promising contender among the active metals, including Ni, Co, Fe, Cu, Rh, Ru, Pt, and Pd, due to its great performance and low price. Over the 10 Ni–CaCO₃ catalyst, 100% conversion of glycerol and ethanol, 92% summed H₂ and CO selectivity, and an H₂/CO ratio of 1.2 could be reached under ideal conditions. Meanwhile, the robustness of this integrated technique was proved over five dry reforming–regeneration cycles. The findings suggest a novel way to use CO₂ in the form of carbonates [47].

2.4. Nickel Catalysts for Glycerol Reforming

The catalyst based on Ni becomes a choice for the reason that the metallic sites of Ni work well enough in water gas shift reaction as well as C–H and C–O cleavage. Nevertheless, the tremendous challenge is how to control catalysts' deactivation triggered by sintering and deposition of carbon at catalyst active sites under optimum operating conditions [13]. Hence, various protocols [40,48] and supports like Al₂O₃ [49–51], ZrO₂ [52–54], CeO₂ [55,56] were generated.

Yancheshmeh et al. suggested a new and simple method for preparing Ni-modified Al₂O₄ spinel catalyst from the steam reforming technique of glycerol for the production of hydrogen. Solvothermal preparation method was used for catalyst represented as NiAl-G1, and the coprecipitation preparation method was used for catalyst described as NiAl-G2 as well as NiAl-C (NiAl₂O₄ catalyst synthesized via the coprecipitation method was designated as NiAl-C). The maximum hydrogen yield was 76.38% achieved with 95.42% maximum glycerol transformation on NiAl-G2 catalyst 630 °C, 1 atm, and 19,600 cm³/g_{cat}/h space velocity reaction conditions. By creating an oxidative environment surrounding nickel active sites, the creation of a well-dispersed CeAlO₃ phase slowed the growth of filamentous carbon on the nickel surface and aided the gasification of carbon deposits. During the 16-h SRG process, the catalytic activity was maintained, and the rate of coke generation was as low as 0.0004 g_{coke}/g_{cat}h⁻¹. These findings support Ce/NiAl-G2's potential as a catalyst for the SRG reaction [56]. Ni added to CaO-modified attapulgite (CaO–ATP) catalyst from reforming of glycerol for hydrogen manufacturing. Using the impregnation technique, Ni–Al₂O₃, Ni–ATP, and Ni–CaO–ATP catalysts can be synthesized. A maximum hydrogen yield of 85.3% was achieved on Ni–CeO–ATP catalyst with 93.71%

glycerol conversion at $T = 600\text{ }^{\circ}\text{C}$ and $\text{GHSV} = 1\text{ h}^{-1}$ reaction condition. The stability of catalyst showed that ATP had better resistance for deposition of carbon compared to alumina and CaO addition further reduced the production of carbon. Due to its unusual intermediate structure, ATP outperformed Al_2O_3 as a carrier. When CaO was utilized as an ATP modifier, it promoted the water gas shift reaction, resulting in increased hydrogen yield, hydrogen selectivity, and a reduction in CO production. The stability results revealed that ATP is more resistant to carbon deposition than Al_2O_3 , and the addition of CaO lowered carbon formation even more. As a result, a Ni-based catalyst supported on a CaO-modified attapulgite could be a potential material for efficient glycerin steam reforming to create H_2 [57].

Wu et al. explored the mesoporous Ni-Cu/ CeO_2 for the production of renewable hydrogen via APR of glycerol. The C-C breakage of glycerol benefits from Ni, but Cu can amplify the WGS reaction. Cu metal's surface is amenable to adsorption Carbonyl radical following glycerol's decarbonylation and hydroxyl free radical in the solution, which facilitates the reaction. Consequently, the addition of Cu element enhanced the proportion of H_2 and CO_2 in the overall gas. It was discovered that increasing the catalyst's Cu concentration improved hydrogen production (125.08 to $195.57\text{ }\mu\text{mol min}^{-1}\text{ g}_{\text{cat}}^{-1}$). Additionally, the CO_2 in overall gas was absorbed by the addition of CaO and it lowers the activation energy. Hence, $1\text{Ni}2\text{Cu}/\text{CeO}_2 + 0.2\text{gCaO}$ catalyst shows H_2 production rate increased from 168.97 to $301.92\text{ }\mu\text{mol min}^{-1}\text{ g}_{\text{cat}}^{-1}$. Therefore, improved H_2 production as a result of the inclusion of Cu and CaO [29].

Liu et al. studied MgO supported Ni-Co bimetallic catalyst prepared by sol-gel method followed by calcination. The resulted catalyst examined the APR of glycerol for hydrogen production. After addition MgO support, H_2 production activity improves by 1.5 times compared to pure Ni-Co bimetallic catalyst. Due to the in-situ adsorption and removal of CO_2 , the WGS reaction was further stimulated with the addition of CaO, and the methanation reaction was inhibited, resulting in the catalyst having a high activity of hydrogen production. The stability test also shown that the gelatinous MgO supports had an impact on the catalyst's activity and stability [30].

Veiga et al. studied crude glycerol steam reforming with oxalic acid to synthesize Ni-doped La-Zr catalysts. Ni-doped La-Zr catalyst was prepared with the coprecipitation method at different calcination temperatures. Ni-doped La-Zr catalysts calcined at $850\text{ }^{\circ}\text{C}$ achieved 90% hydrogen yield and 99.9% glycerol conversion. The catalyst prepared at $850\text{ }^{\circ}\text{C}$ calcination and operated at $650\text{ }^{\circ}\text{C}$ reaction showed higher catalytic stability, activity, and better resistance to carbon formation. The greatest performance seen for Ni-850 catalysts is mostly due to the development of oxygen vacancies caused by nickel substitution into the La-Zr lattice during calcination, favoring the oxidation of carbon deposits throughout the process [58].

Charisiou et al. investigated Ni supported over $\text{Y}_2\text{O}_3\text{-ZrO}_2$ catalyst for the glycerol steam reforming. The catalyst synthesized through the impregnation technique was Ni modified Zr and Ni modified YZr. The maximum transformation was 90% achieved at $700\text{ }^{\circ}\text{C}$, and the maximum H_2 selectivity was 82% achieved at $450\text{ }^{\circ}\text{C}$ over Ni modified YZr catalyst. The research on spent catalyst revealed the less carbon deposition on Ni/Zr (Ni modified Zr) catalyst as it was more graphitic in nature and higher carbon deposition on Ni/YZr spent catalyst. The addition of Y_2O_3 stabilized the ZrO_2 tetragonal phase, resulted in more easily reducible NiO nanoparticles, increased the O_2 storage capacity of the support and the medium strength acid sites of the catalyst, and, despite having a higher concentration of basic sites, the Ni/YZr presented more stable monodentate carbonates. Allyl alcohol, acetaldehyde, acetone, acrolein, acetic acid, and acetol were the primary liquid products detected for both catalysts. Although higher amounts of carbon were deposited on the Ni/YZr spent catalytic sample ($0.70\text{ g}_{\text{coke}}/\text{g}_{\text{catal}}$ compared to $0.51\text{ g}_{\text{coke}}/\text{g}_{\text{catal}}$ for the Ni/Zr catalyst), the addition of Y_2O_3 on to the ZrO_2 support resulted in structures with lower crystallinity (amorphous carbon) that are more easily oxidized during the reaction. The coke deposits found on spent Ni/Zr catalysts, on the

other hand, were graphitic structures with little flaws, resulting in the deadly encapsulation of Ni particles [54].

2.5. Cobalt Catalysts for Glycerol Reforming

Cobalt (Co) played an extensive role in the synthesis of hydrogen as many researchers represented this glycerol steam reforming. Ghungrud and Vaidya studied the synthesis of hydrogen by sorption-enhanced steam reforming technique (SESGR) on a Co-promoted hydrotalcites catalyst. 92.8% maximum glycerol conversion and 89.7% hydrogen yield were achieved over Co-Ca-HTlc catalyst represented as HM2 at $T = 823$ K, $GHSV = 5600$ mL $g^{-1} h^{-1}$. Ca, Co, and Zn promoted hydrotalcite catalysts were manufactured through the precipitation method. HM2 contained Cu showed the best performance for the dehydrogenation process, and it was known that basic sites promoted the dehydrogenation process. At 550 °C, Cu-bearing materials showed a long pre-breakthrough duration (40 min) and high H_2 purity (93.1 mol%). They were also better adsorbents, removing 1.1 mol CO_2/kg sorbent at 550 °C. Over 20 cycles of adsorption and regeneration, the cyclic stability of materials was examined. The potential of customized HTlc-materials for better H_2 production from the SESGR process is explored in this work [59].

A feasible reaction pathway for the SESGR process was provided based on the product composition (Figure 3). Glycerol undergoes dehydration hydrogenation reactions upon adsorption, resulting in acetaldehyde. The adsorbed acetaldehyde was then further hydration-dehydrogenated into acetic acid. Over Co metal, acetic acid undergoes C-C bond breakage, yielding H_2 , CO_2 , CO , and CH_4 . The basic catalyst promotes rapid dehydrogenation, which prevents the generation of olefins and carbon deposition. CO and CH_4 are converted to H_2 and CO_2 by WGS reaction and steam reforming processes, with trace amounts of CO remaining [59].

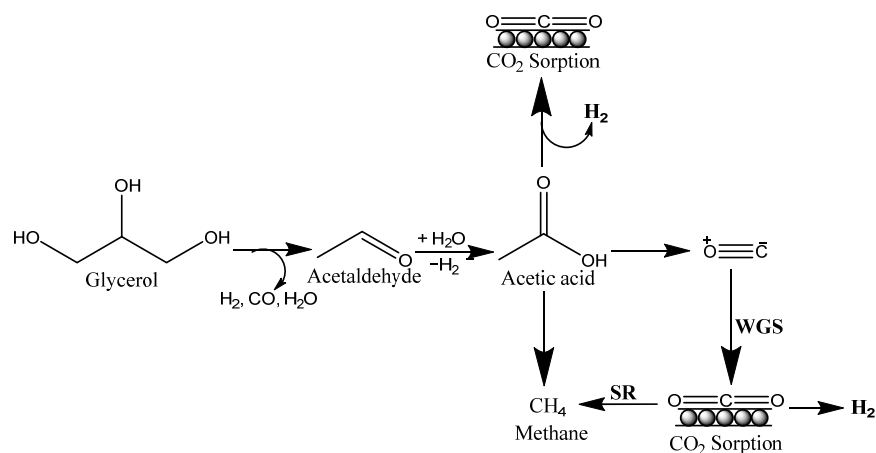


Figure 3. Plausible reaction mechanism for SESGR.

Zhou et al. investigated NiCo modified CNTs bimetallic catalysts with an appropriate distribution of Ni, as well as Co, metal for synthesizing hydrogen through the impregnation technique in which metal precursors were injected into the cave of CNTs by ultra-radiations. At 450 °C and 1 atm, 100% glycerol transformation was achieved with 91.4% H_2 selectivity over Ni(i)Co(i)/CNTs catalyst. Ni(i)Co(i)/CNTs exhibited the best stability and catalyst performance. Although the Ni and Co oxides were only partially reduced, the location of metal species had a significant impact on reducibility. The synergistic effect between Ni and Co species was found in Ni(i)Co(i)/CNTs and Ni(o)Co(o)/CNTs, where they had the same distribution on the internal or external wall. Sintering of active sites was markedly simpler on the external wall of CNTs, causing the catalyst to deactivate quickly and become less reactive for the water gas shift process. The result of this study revealed that there is a new and straightforward method for assembling bimetallic catalyst systems. The Ni-based bimetallic catalysts might be used to reform mono/multi-alcohols such as ethanol, ethylene

glycol, sorbitol, and other organic wastes from second-generation biorefineries, as well as biogas and other organic wastes [37].

Al-Salihi et al. investigated Co-Ni-MgO-based SBA-15 nano-catalysts for the glycerol steam reforming for hydrogen manufacturing. The one pot hydrothermal method was used to create different mesoporous catalysts, such as Co-SBA-15, Ni-SBA-15, Co-MgO-SBA-15, Ni-MgO-SBA-15, and Co-Ni-SBA-15 and bimetallic 10 wt.% Co-5 wt.% Ni modified SBA-15 catalyst synthesized by the impregnation method. A glycerol conversion rate of 100% along with 82.8% hydrogen selectivity was achieved over 10 wt.% Co-5 wt.% Ni modified SBA-15 catalyst at 650 °C. At a low temperature (450 °C), the one-pot catalysts showed 50% glycerol conversion compared to 70% for the impregnated catalyst, while both yielded 62% H₂ selectivity. Cobalt-based SBA-15 catalysts have superior GSR activity and stability than nickel-based catalysts in monometallic catalysts. The addition of MgO to Co-SBA-15 improved glycerol conversion (up to 99%) and catalyst stability. The addition of MgO to Ni-SBA-15 reduced the quantity of carbon deposition on the catalysts by as much as 66%, according to TGA-TPO analyses of spent catalysts. It's worth noting that under our experimental conditions, all of the catalysts examined at the optimum temperature of 650 °C demonstrated a remarkable hydrogen selectivity of 70% [36].

Duo et al. developed chemical looping steam reforming process for glycerol conversion to hydrogen over Al-MCM-41 and SBA-15 well-order mesoporous OCs containing NiO and CeO₂ nanoparticles [33]. It was discovered that the NiO and CeO₂ in the OCs were reduced by glycerol, and the reduced OCs were in charge of producing hydrogen. It was shown remarkable stability in 60 redox cycles (180 h), and the carbon conversion and hydrogen selectivity were both over 60% and 85%, respectively. Oxygen transport was enhanced by heavily loading mesoporous MCM-41 and SBA-15 with NiO and CeO₂, which also produced outstanding redox CLSR cycles and long-term stability [33].

The summary of some more reported literature related to glycerol reforming over various catalysts to produce hydrogen is represented in Table 2. Noble metal catalysts, such as Pd, Ru, Ir, Rh, and Pt, are known for their high catalytic activity, which results in good performance and coke resistance. Other catalysts, such as Ni, Co, and Cu, on the other hand, are less expensive and more readily available and have a desirable catalytic activity for boosting hydrogen production. Their stability, on the other hand, is undesirable since the coking process frequently deactivates them. As a result, developing a highly active and stable catalyst requires the employment of metals as catalysts in combination with the proper selection of support (based on porosity, redox characteristics, and thermal stability, among other factors). Alumina and silica are the most common catalytic supports in research, but some catalysts can also be supported on active carbon, nanotubes, mesoporous carbon, nanoparticles, and other materials. Due to its high specific surface and thermal stability, alumina is the preferred and most used support for this purpose. However, carbon deposition tends to render it inactive. The optimal bimetallic catalyst must possess excellent thermal strength, mechanical resistance, and redox characteristics to produce H₂ with high selectivity.

Table 2. Hydrogen production from glycerol reforming using various catalytic systems under optimal reaction conditions.

S. No.	Catalyst	Reaction Condition/Reactor	X (%)	S (%)	Y (%)	References
1	Co-Ni-MgO-based SBA-15 (one-pot hydrothermal and impregnation method)	T = 650 °C P = 1 atm (Fixed bed reactor)	100	82.8	82.8	[36]
2	Pt and/or Ni supported over γ -alumina (Sol-gel method)	T = 250 °C P = 30 bar WHSV = 2.6 h ⁻¹	100	-	-	[37]

Table 2. Cont.

S. No.	Catalyst	Reaction Condition/Reactor	X (%)	S (%)	Y (%)	References
3	Pt and Ni supported SiO ₂ (Ion exchange method)	T = 350 °C P = 1 atm Feed flowrate = 0.5 cm ³ h ⁻¹ (Fixed bed reactor)	100	70	70	[38]
4	Ru doped Al ₂ O ₃	T = 500 °C, P = 0.1 MPa Cat. Wt. = 0.1 g W/FAO = 1.98	89.1	-	-	[41]
5	CeZr-CoRh	T = 650 °C, P = 0.1 MPa Cat. Wt. = 55 mg WHSV = 8.4 g _{gly} g _{cat} ⁻¹	100	86	86	[44]
6	Rh modified MeAl ₂ O ₄ at Al	T = 723 K WHSV = 34,000 mL g ⁻¹ h ⁻¹	100	-	-	[45]
7	Rh/Al ₂ O ₃ (Impregnation technique)	T = 823 K WHSV = 4.8 × 10 ³ N mL/g _{cat} min	100	-	-	[46]
8	Ni/CaCO ₃	T = 550 °C P = 1 atm	100	92	92	[47]
9	Rh/γ-Al ₂ O ₃ @CeO ₂ , MgO, La ₂ O ₃ (Co-precipitation method)	T = 600 °C P = 1 atm GHSV = 5000 N mL g ⁻¹ hr ⁻¹ (Fixed bed reactor)	90	78	78	[49]
10	Ni supported over Y ₂ O ₃ -ZrO ₂ (Impregnation technique)	T = 700 °C	90	91	82	[54]
11	Ni modified Al ₂ O ₄ (Cociprecipitation method)	T = 630 °C P = 1 atm press., WHSV = 19,600 cm ³ /g _{cat} /h	95.42	80	76.4	[56]
12	Ni added to CaO—modified attapulgite (Impregnation method)	T = 600 °C Cat. Wt. = 0.5 g GHSV = 1 h ⁻¹	93.7	91	85.3	[57]
13	Co promoted hydrotalcite (Precipitation method)	T = 550 °C GHSV = 5600 mL g ⁻¹ h ⁻¹	92.8	96.7	89.7	[59]
14	NiCo modified CNTs bimetallic catalysts (Impregnation method)	T = 450 °C P = 1 atm (Fixed bed reactor)	100	91.4	91.4	[60]
15	Pt/Al ₂ O ₃	T = 200–240 °C P = 16–33.5 bar (Batch reactor)	84	16.8	14.1	[61]
16	Pt/Al ₂ O ₃	T = 240 °C P = 42 bar (Batch reactor)	34	36.8	12.5	[62]
17	Pt/SiO ₂ (Sol—gel method)	T = 300–400 °C P = 1 atm (Microchannel reactor)	96.8	90	89.7	[63]

Table 2. Cont.

S. No.	Catalyst	Reaction Condition/Reactor	X (%)	S (%)	Y (%)	References
18	Pt/ γ -Al ₂ O ₃ , SiO ₂ & silica—alumina (Impregnation method)	T = 225 °C P = 29 bar WHSV = 4.2 h ⁻¹ (Fixed bed reactor)	11.9	73	8.9	[64]
19	Pt/ZrO ₂ (Impregnation method)	T = 350 °C P = 29 bar (Fixed bed reactor)	100	69	6.9	[65]
20	Pt/Al ₂ O ₃ , Puralox, Catapal B (Impregnation method)	T = 250 °C Cat. Wt. = 300 mg Feed flowrate = 0.5 mL/min (Fixed bed reactor)	57	-	85	[66]
21	Pt—Re/C (Impregnation method)	T = 225 °C P = 420 psi WHSV = 5 hr ⁻¹ (Fixed bed reactor)	89.4	26.1	23	[67]
22	10 Ni/Al ₂ O ₃ /5 CeO ₂ (Impregnation method)	T = 550–800 °C P = 1 atm WHSV = 10 hr ⁻¹ (Fixed bed reactor)	100	88.6	86	[68]
23	Ru-Mg-Al hydrotalcite- mixed oxides (Impregnation method)	T = 400–700 °C P = 1 atm GHSV = 69,000 h ⁻¹ (Fixed bed reactor)	45	90	40.5	[69]
24	Ru/Al ₂ O ₃ (Wet co-impregnation method)	T = 400–600 °C P = 1 atm Cat. Wt. = 200 g W/F = 1.05 mg min mL ⁻¹ (Fixed bed reactor)	100	80	80	[70]
25	Ru/C (Impregnation method)	T = 773 K P = 1 atm (Fixed bed reactor)	94.6	99.8	94.5	[71]
26	Mg(Al)O/Ru (Impregnation method)	T = 450–650 °C P = 1 atm (Fixed bed reactor)	97	96	90	[72]
27	C/Pt and Pt/Ru (Impregnation method)	T = 225 °C P = 1 bar (Fixed bed reactor)	24	-	-	[73]
28	Rh/ZrO ₂ , Rh/CeO ₂ (Impregnation method)	T = 650–750 °C Cat. Wt. = 20 mg (Fixed bed reactor)	79	30.6	24.2	[74]
29	Rh/Al ₂ O ₃ (Impregnation method)	T = 250 °C P = 50 bar Cat. Wt. = 250 mg WHSV = 2.45 h ⁻¹ (Fixed bed reactor)	82	85.2	69.9	[75]
30	Pt and Pt-Rh/ α -Al ₂ O ₃ (Impregnation method)	T = 503 K Cat. Wt. = 300 mg (Batch reactor)	67	1.67	1.12	[76]

Table 2. Cont.

S. No.	Catalyst	Reaction Condition/Reactor	X (%)	S (%)	Y (%)	References
31	Rh and Ni/ γ -Al ₂ O ₃ (Impregnation method)	T = 723 to 1073 K P = 1 atm GHSV = 5000 to 30,000 mL _{gly} h ⁻¹ mL _{cat} ⁻¹	69	50	34.5	[77]
32	Ni-La-Ti oxide (Coprecipitation method)	T = 500–650 °C P = 1 bar Cat. Wt. = 0.1 gm WHSV = 3 h ⁻¹ (Fixed bed reactor)	99.7	90.3	90	[78]
33	NiAl ₂ O ₄ (Impregnation method)	T = 600 °C Feed flowrate = 2.5 mL/h (Fixed bed reactor)	99	98.9	98	[79]
34	La-promoted Ni/Al ₂ O ₃	T = 923–850 °C P = 1 atm WHSV = 3.6 × 10 ⁴ mL ⁻¹ h ⁻¹ (Fixed bed reactor)	96	98.9	95	[80]
35	La _{1-x} Ca _x NiO ₃ perovskite-oxides (Impregnation method)	T = 550 °C P = 1 atm Cat. Wt. = 200 mg WHSV = 2.5 hr ⁻¹ (Fixed bed reactor)	100	80	80	[81]
36	Ni and Ni—Co/alumina (Impregnation method)	T = 300–700 °C P = 1 atm WHSV = 10 hr ⁻¹ (Fixed bed reactor)	-	-	83	[82]
37	Ni/ α -Al ₂ O ₃ and α -Al ₂ O ₃ modified by ZrO ₂ and CeO ₂ (Impregnation method)	T = 600 °C P = 1 atm Feed flow rate = 0.022 cm ³ min ⁻¹ (Fixed bed reactor)	90	95.6	86	[83]
38	LaNiO ₃ and LaCoO ₃	T = 700 °C P = 1 atm (Fixed bed reactor)	100	98	98	[84]
39	0.25 CoAl, 0.625 CoAl Co ₃ O ₄	T = 260 °C P = 5 MPa WHSV = 24.5 h ⁻¹ (Fixed bed reactor)	98	29	10	[85]
40	Co-Ce/Hap (Impregnation method)	T = 750 °C P = 1 atm (Fixed bed reactor)	99	79	7.2	[86]
41	Co/SBA-15 with Zr, Ce and La (Impregnation method)	T = 500–600 °C P = 1 atm WHSV = 7.7 h ⁻¹	100	72	72	[87]
42	La _x -Ce _y -CoO ₃ (Co—precipitation method)	T = 700 °C P = 1 atm (Fixed bed reactor)	100	68	68	[88]
43	Co/Al ₂ O ₃ (Impregnation method)	T = 723–923 K P = 1 atm GHSV = 5 × 10 ⁴ mL g _{cat} ⁻¹ h ⁻¹ (Fixed bed reactor)	65	80	52	[89]

Table 2. Cont.

S. No.	Catalyst	Reaction Condition/Reactor	X (%)	S (%)	Y (%)	References
44	Ceria/Ir, Co and Ni (deposition—precipitation method)	T = 250–600 °C P = 1 atm GHSV = 11,000 mL g _{cat} ⁻¹ h ⁻¹ (Fixed bed reactor)	100	85	85	[90]

X = Conversion, S = Selectivity, Y = Yield.

3. Glycerol Dehydration

Acrolein was obtained by anhydrous glycerol decomposition in the existence of solid catalysts such as alkali–metal acid sulfates and phosphorus pentoxide in the 19th century [91,92]. Hence, the suggested route is illustrated in Figure 4. Acrolein is transformed directly into targeted high-value-added derivative products because of its toxic effects. Acrolein is an intermediate in producing acrylic acid and acrylic polymers in the industry. The consumption of acrolein is also for the production of DL-methionine, and 3-methylthio-propionaldehyde is produced as an intermediate here [93]. Early studies concentrated on homogeneous catalysts in the aqueous phase under near- or supercritical conditions. However, the vapor phase over heterogeneous catalysts are chosen due to the predicted high cost of the reaction vessel and separation concerns [10]. However, until the end of the twentieth century, when cheaper glycerol from the biodiesel synthesis process became accessible, these early works in both the gaseous and liquid phases remained unexplored [93].

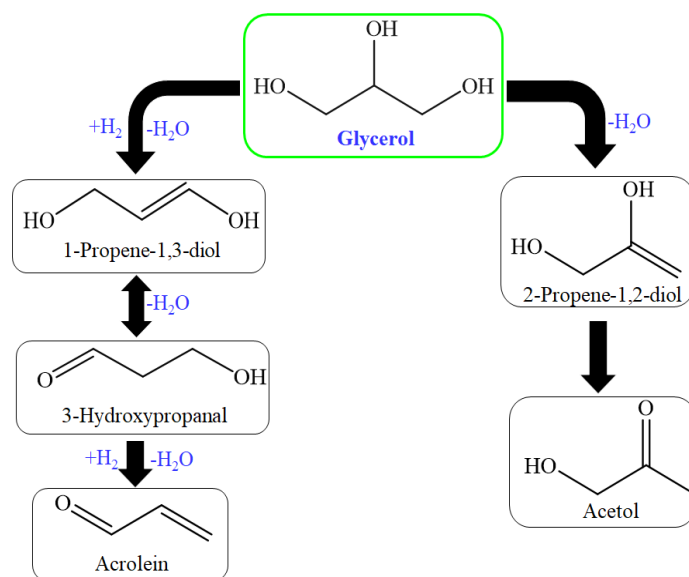


Figure 4. Reaction route for glycerol dehydration to produce acrolein and acetol.

The high selectivity was achieved due to the control of 1st dehydration reaction. Tsukuda et al. proposed this mechanism, where 3-hydroxypropionaldehyde formation was favorable over the acetol formation, which is considered a byproduct of the primary reaction step; further, this mechanism (Figure 5) suggested two hydrogenation steps: first from acrolein and second from acetol to achieve allylic alcohol and 1,2-PDO, simultaneously [94,95]. So many solid acid catalysts have been used for dehydration of glycerol for acrolein production through zirconia, heteropoly acid, niobia, and alumina catalysts [96–98].

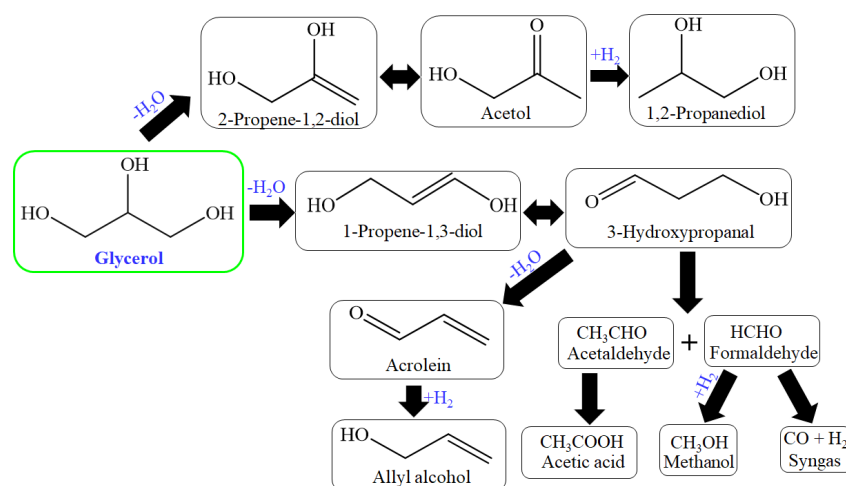


Figure 5. Reaction route for acrolein formation by acid-base catalysts.

3.1. Zeolite Catalysts for Glycerol Dehydration

Lin et al. investigated β zeolites (HNa- β - κ) for the production of acrolein through glycerol dehydration. In total, 65% glycerol transformed to produce 23.3% acrolein yield at HNa- β -0 catalysts at 200 °C. It was speculated that smaller pores increased selectivity but reduced activity for acrolein production. An increase in temperature favored the selectivity of acrolein. After being employed in the reaction test (see *infra*) and recalcination at 450 °C in the air for 4 h, the XRD patterns of these zeolitic catalysts were substantially identical. These results showed that the ion-exchange technique, subsequent calcination, and reaction tests did not result in any visible changes in the zeolitic crystal structure. As the Na/Al ratio increased, the apparent surface area of the HNa- β - κ zeolites decreased. At the same time, the pore width reduced as the Na⁺/Al ratio increased, which could explain why Na⁺ is larger than H⁺ when residing in the zeolitic channel. According to the pore diameter data, these pore widths correspond to the 12-membered ring in the β -zeolites and the 10-membered ring in the H-MFI zeolite. Na⁺/H⁺ ratio increment also enhanced acrolein selectivity and decreased glycerol conversion. The highest acrolein yield was achieved due to the replacement of acidic sites with non-active Na⁺ sites [99].

Ren et al. investigated MnHPO₄ and meso-zeolite (H-ZSM-5) catalyst prepared by the ion-exchange technique and concluded that the less strong acid amount was more beneficial for the production of acrolein and also coke suppressed in glycerol dehydration. A 100% transformation of glycerol was achieved for all reactions and 84.7% highest acrolein yield over meso-zeolite(HZSM-5) supported on MnHPO₄ catalysts [100]. Meso and microporous zeolite by one-step synthesis technology for acrolein formation from glycerol dehydration. HZSM-25 catalyst achieved 99% glycerol transformation and 80% acrolein selectivity at 450 °C, 1 atm, and 38.47 h⁻¹ WHSV. The high acidity and fast diffusion of species in synthesized ZSM-5 supported acrolein production from dehydration of glycerol. Diffraction peaks of five types of transition metal hydrogen phosphates supported on meso-HZSM-5 were also shown to exhibit this behavior [101]. Qureshi et al. investigated nano H-ZSM-5 highly crystalline catalyst for glycerol dehydration through hydrothermal technique. A 98% glycerol transformation occurred to produce 87% acrolein selectivity at HZSM-5 (Si/Al = 75) at 320 °C, 1 atm, and 4 h⁻¹ WHSV. According to these findings, the catalysts with a Si/Al ratio of 75–100 had a higher crystallinity than the other samples. The SEM pictures revealed the catalyst's surface morphology, particle size, and crystal aggregation. The exterior surface of all H-ZSM-5 catalysts produced was uniform and had a highly orientated shape. The catalysts exhibit consecutive crystal lattices and a smooth surface, according to TEM pictures of H-ZSM-5 with a Si/Al ratio of 75 [102].

Yun et al. investigated marigold-like silicon dioxide (silica) functionalized through groups of sulfonic acid (MF-FS) and zeolite (HZSM-5) catalysts for the production of acrolein from glycerol dehydration. The maximum acrolein yield was 73%, with 100%

glycerol transformation achieved over MF-CS catalyst at 250 °C. Bronsted acid sites in MF-FS catalyst promoted stability as well as selectivity for acrolein production [103]. Chai et al. studied acrolein production through dehydration on various solid acid-base catalysts synthesized by the impregnation method. A 100% glycerol transformation was achieved with 65% acrolein selectivity over 15 wt.% WO_3/ZrO_2 catalyst at 315 °C, 1 atm, and 80 h⁻¹ GHSV. For acrolein production, Bronsted acidic sites were superior to Lewis acidic sites [94]. Xie et al. investigated microwave absorbing catalysts for acrolein production from glycerol dehydration. Most notably, the catalyst stability by microwave heating technique was much better than the heating process by electric. WO_3/ZrO_2 at SiC coated microwave absorbing catalyst was synthesized. The complete glycerol transformation (100%) was achieved with 70% acrolein selectivity by 250 °C microwave heating [104].

Shan et al. investigated fabricated nanosheet MFI zeolite catalyst for glycerol dehydration for acrolein production [105]. A 99.7% transformation of glycerol was achieved with 81.8% acrolein at 320 °C and 1 atm. Compared to conventional ZSM-5 zeolite (CMZ-X), MFI zeolites nanosheets were more active as well as stable for glycerol dehydration reaction in the gas phase. The nanosheet MFI zeolites (NMZ-X) decreased the rate of coke deposition which resulted higher stability as well as activity. The zeolites in CMZ-X produced with tetrapropylammonium hydroxide as the structural guiding agent were shown as uniform 400 nm particles with cylindroid intergrowth. The NMZ-X Si/Al molar ratio has a significant impact on the morphologies of nanosheet MFI zeolites. NMZ-100 appears to be a three-dimensional multi-lamellar stacking of MFI nanosheets with intergrowth. The NMZ-100 particles had a diameter of roughly 1.5 µm and were made up of 30–40 nm thick lamellar stacking. Meanwhile, NMZ-50 demonstrated similar MFI nanosheet lamellar stacking, but the particle size (500 nm) and lamellar stacking thickness (approximately 10 nm) were substantially less. NMZ-30, on the other hand, looks like cotton balls and could not tell the MFI nanosheets from the SEM image. NMZ-30 was well-crystallized and exhibited nanosheet MFI zeolite properties, as indicated by the XRD patterns. It was discovered that Al content had a crucial impact on the development of NMZ-X by comparing TEM pictures of nanosheet MFI zeolites with varied Si/Al molar ratios. Due to the abundance of unstable Si–O–Al units, it was difficult to generate large area MFI nanosheets with a low Si/Al molar ratio [105].

3.2. Titania Catalysts for Glycerol Dehydration

Titanium oxide (Titania) has three crystalline phases: brookite, anatase, and rutile. Among all, the anatase phase has vital applications [106–109]. Babaei et al. investigated TiO_2 catalysts for acrolein production for glycerol dehydration. It was mentioned that the central hydroxyl group adsorption on the surface had the best geometry and energy (30.91 kcal/mol) for dehydration reaction to acrolein. The glycerol dehydration to acrolein is followed by removing water molecules. The TiO_2 surface exhibited more activity in proton transfer reaction with 89.1 kcal/mol E (activation energy) comparing the above two routes for acrolein formation [109]. Ulgen et al. synthesized WO_3/TiO_2 catalyst through the impregnation method for acrolein formation from glycerol dehydration. Maximum acrolein selectivity of 80% and the complete conversion of glycerol was achieved over WO_3/TiO_2 catalyst at 280 °C. In most cases, a larger BET surface area was associated with better glycerol conversion. Titania-supported tungsten oxide systems were ideal catalysts for the dehydration reaction of glycerol due to their longer service time, decreased deactivation speed, and much lower pricing [110].

3.3. Silica Catalysts for Glycerol Dehydration

Wang et al. focused on low-temperature (210–230 °C) glycerol dehydration to acrolein through temperature-programmed surface reaction (TPSR). A series of acid catalysts (Lewis acid catalysts, supported heteropolyacids and superacids, molecular sieves, and metal oxides) synthesized by the impregnation method has been screened for glycerol dehydration at low temperature (210 °C) through TPSR. SiW/SiO_2 , as well as $\text{SO}_4^{2-}/\text{TiO}_2$

achieved high acrolein selectivity (85% and 86%) simultaneously. The maximum glycerol transformation was achieved at 94.4% at 230 °C [111]. Rosas et al. investigated some most active catalysts, namely, NH_4 and La modified β zeolites, Pd and La modified Y zeolites, hierarchical zeolite (ZSM-5), WO_3 modified ZrO_2 , WO_3 modified TiO_2 , ZrO_x and WO_x modified NbO_x , WO_3 - SiO_2 modified ZrO_2 , NbO_x - WO_x modified Al_2O_3 , H_3PO_4 modified MCM-41, SAPO-40, and NbPSi for glycerol dehydration reaction in the gas phase. A 100% conversion was obtained at 300–325 °C. In this, the gas-phase catalytic process was more suitable than the liquid-phase due to high acrolein yields (>70%) [112]. Silica and phosphate supported copper catalyst for glycerol dehydration to produce acetol. Silica and phosphate supported copper catalyst produced through sodium silicate neutralization with the orthophosphoric acid and added copper nitrate. After this, 58.3% acetol selectivity and 100% glycerol transformation were achieved 40 CuSP catalyst at 220 °C, and atmospheric pressure. Lewis acidic sites were responsible for the increase in selectivity of acetol [113]. Basu et al. investigated silica-supported copper chromite catalyst synthesized through a sol-gel technique for dehydration of glycerol for acetol production. The transformation of glycerol reached 100% with 70% maximum selectivity of acetol for 40 wt.% Copper chromite loading on silica at 220 °C and atmospheric pressure. The spent and oxidized catalyst presented lower selectivity and conversion compared with reduced form catalyst due to cupric ion in reduced form catalyst, which worked as Lewis acid sites in dehydration [114].

3.4. Alumina Catalysts for Glycerol Dehydration

Mesoporous alumina was prepared with different precipitants through a continuous precipitation method for gas-phase glycerol dehydration for acrolein production by Lima et al. A 99% glycerol transformation occurred at alumina catalyst prepared at 7 pH with NaOH precipitant at 500 °C. Results revealed high carbon formation and higher olefins production, which showed the production of carbon is related to these by-production formations. The sample synthesized with KOH had the largest specific surface area ($432 \text{ m}^2 \text{ g}^{-1}$) among the influences of the precipitating agent, whereas the sample created with Na_2CO_3 had the lowest specific surface area ($432 \text{ m}^2 \text{ g}^{-1}$) ($48 \text{ m}^2 \text{ g}^{-1}$). The specific surface area of the produced material was similarly affected by the pH of the precipitation. Due to the type of precipitate generated, samples prepared at pH 5 ($389 \text{ m}^2 \text{ g}^{-1}$ of Na_2CO_3 precipitant and $359 \text{ m}^2 \text{ g}^{-1}$ of NaOH) have a greater specific surface area than those prepared at pH 7. When precipitation was carried out at pH 7, the resulting residue was weakly crystalline, creating pseudo-boehmite. At pH 5, an amorphous precipitate was formed, yielding a microcrystalline boehmite with a higher specific area [115].

Kim et al. investigated silica and alumina catalyst for glycerol dehydration reaction in gas-phase for production of acrolein. The conversion of glycerol was 50% along with 16% acrolein selectivity achieved over $\text{Si}_{0.6}\text{Al}_{0.4}\text{O}_x$ catalyst at 315 °C and 62 h^{-1} WHSV. It was concluded that the yield of acrolein depended on the brønsted acid sites. As Si mole fraction was increased up to 0.8, the intensity of the Al_2O_3 XRD peak increased and subsequently declined as Si mole fraction was increased. Due to the tetrahedral interaction between Al and SiO, the degree of crystallinity is determined by the Al concentration contained in SiO_2 . The specific surface areas of the silica–alumina increased dramatically when Al (or Si) species were added, compared to SiO_2 and $-\text{Al}_2\text{O}_3$. The catalyst pore volume followed a volcano-like pattern in relation to the mole fraction of Al, while the average pore diameter shrank as the mole fraction of Al increased. The catalysts' pore size distributions revealed a noticeable variation in pore diameter with regard to the Al content. For silica–aluminas with Al mole% of less than 0.2, a relatively broad pore size distribution was discovered [116].

A summary of some more reported literature on glycerol dehydration over various catalysts to produce acrolein is represented in Table 3 [92,99–136].

Table 3. Acrolein production from glycerol dehydration using various catalytic systems under optimal reaction conditions.

S. No.	Catalyst	Reaction Conditions/Reactor	X (%)	S (%)	Y (%)	References
1	HPA, H-SiW, H-PW and H-PMo/ γ -Al ₂ O ₃ (Impregnation method)	T = 275 °C P = 1 atm feed flowrate = 1.68 mL/h (Fixed bed reactor)	99	42.1	41.7	[92]
2	β zeolites (HNa- β - κ)	T = 200 °C Cat. Wt. = 1 g Feed flowrate = 12 mL/h (Fixed bed reactor)	65	35.8	23.3	[99]
3	MnHPO ₄ and meso-Zeolite (Ion exchange method)	T = 300 °C Cat. Wt. = 0.5 g Feed flowrate = 0.023 mL/h	100	84.7	84.7	[100]
4	Zeolite (one-step synthesis)	T = 723 K P = 1 atm Cat. Wt. = 80 mg Fee flowrate = 0.05 mL/h	99	80.8	80	[101]
5	HZSM-5 (Hydrothermal Technique)	T = 320 °C P = 1 atm WHSV = 4 h ⁻¹ (Fixed bed reactor)	98	88.8	87	[102]
6	WO ₃ /TiO ₂ (Impregnation method)	T = 280 °C P = 1 atm	100	80	80	[110]
7	Pd/LaY Zeolite	T = 573 K P = 1 atm GHSV = 5933 h ⁻¹ (Fixed bed reactor)	93	94.2	87.6	[112]
8	Silica supported copper chromite (Sol gel method)	T = 220 °C	100	70	70	[114]
9	Zeolite	T = 290–650 °C WHSV = 282–388 hr ⁻¹ (Fluidised bed reactor)	100	62.1	62.1	[117]
10	Sulfated zeolite (Precipitation method)	T = 290–390 °C P = 1 atm GHSV = 18,000–360 hr ⁻¹ (Continuous flow reactor)	49	42	20.58	[118]
11	Na-ZSM-5 and H-ZSM-5	T = 315 °C P = 1 atm Feed flow rate = 23.4 m mol/h (Fixed bed reactor)	75.8	63.8	48.36	[119]
12	ZSM-23, HY, Mor, H and SBA-15, CVD, H β (Impregnation method)	T = 250 °C P = 70 bar (Autoclave with stirrer)	95	18.5	17.58	[120]
13	WO ₃ /TiO ₂ (Sol-gel and solvothermal method)	T = 200–400 °C P = 1 atm WHSV = 22.9 g _{Etol.} g/cat/h (Fixed bed reactor)	88	87.5	77	[121]

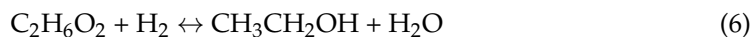
Table 3. Cont.

S. No.	Catalyst	Reaction Conditions/Reactor	X (%)	S (%)	Y (%)	References
14	WO ₃ /TiO ₂	T = 280 °C P = 1 atm (Fixed bed reactor)	95	73	69.4	[122]
15	WO _x /TiO ₂ Sand NbO _x /TiO ₂	T = 400 °C P = 25 and 33 MPa (Fixed bed reactor)	100	80	80	[123]
16	HPW/TiO ₂ (Impregnation method)	T = 280 °C P = 1 atm GHSV = 4400 h ⁻¹ (Fixed bed reactor)	100	74	74	[124]
17	Al ₂ O ₃ -, SiO ₂ -, and TiO ₂ - /Nb- and W-oxide (Impregnation method)	T = 305 °C P = 1 atm (Fixed bed reactor)	100	66.2	66.2	[125]
18	H ₆ P ₂ W ₁₈ O ₆₂ /MCM-41-SUP (Supercritical Impregnation method)	T = 320 °C P = 1 atm Cat. Wt. = 0.5 g WHSV = 0.6 h ⁻¹ (Fixed bed reactor)	94	72	67.7	[126]
19	Al doped SBA-15 (post synthesis method)	T = 325 °C P = 1 atm Feed flowrate = 0.1 mL/hr (Fixed bed reactor)	100	31	31	[127]
20	WO ₃ /Zr Doped Mesoporous SBA-15	T = 325 °C P = 1 atm (Fixed bed reactor)	97	42.3	41	[128]
21	Silica-Supported Phosphotungstic Acid (sol-gel method)	T = 280 °C P = 1 atm (Fixed bed reactor)	99	30	27	[129]
22	Tungsten oxides dispersed on Al ₂ O ₃ , ZrO ₂ , and SiO ₂	T = 315 °C P = 10 kPa GHSV = 400 h ⁻¹ (Fixed bed reactor)	98	70	68.6	[130]
23	Bulk, nanorod and MOF-derived γ-Al ₂ O ₃ ,	T = 240–340 °C WHSV = 2.4 h ⁻¹ (Fixed bed reactor)	80	74	59.2	[131]
24	Pt/γ-Al ₂ O ₃ (Impregnation method)	T = 375 °C P = 1 atm feed flowrate = 12 mL/h (Continuous flow reactor)	90	65	58.5	[132]
25	ZrO ₂ & Ceria/Alumina	T = 300 °C GHSV = 12,000 h ⁻¹ (Micro reactor)	100	85	85	[133]

4. Glycerol Hydrogenolysis

The catalytic hydrogenolysis reaction is completed in two steps: hydrogenation and dehydration. Such a type of reaction system depends mainly on one catalyst particle size along with its structure [134,135]. Fan et al. concluded that the glycerol conversion would be more promising when using an enzymatic approach for glycerol to 1,3-PDO [136]. Sun et al. studied glycerol hydrogenolysis to produce C₃ products such as 1,2-PDO and

1,3-PDO [137]. The reaction route for glycerol hydrogenation producing ethylene glycol, methanol, ethanol, and methane [61]:



The reaction route for glycerol hydrogenation into propylene glycols (1,2-propanediol (1,2-PDO), and 1,3-propanediol (1,3-PDO)) were shown as (Figure 6) [138]. So many heterogeneous catalysts were utilized for hydrogenolysis reaction in which noble metals (Au, Rh, Pd, Pt, and Ru) based catalysts were utilized or non-noble metals (Ni, Co, and Cu) based catalysts were used [139–153].

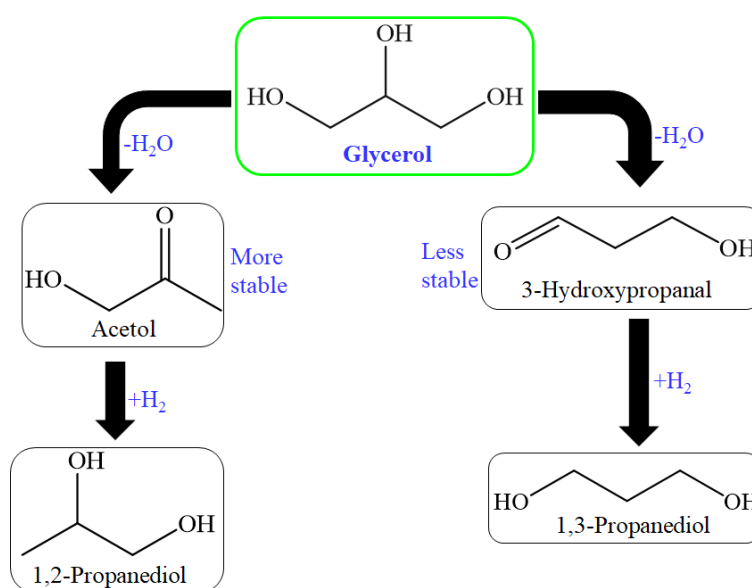


Figure 6. Production of 1,2-PDO and 1,3-PDO through dehydration and hydrogenation of glycerol.

4.1. Nickel Catalysts for Glycerol Hydrogenolysis

Bulk Ni phosphide catalyst prepared through hydrothermal method for glycerol hydrogenolysis for production of 1,2-PDO. 95% 1,2-PDO selectivity along with 5.4% glycerol conversion was achieved over Ni_3P catalyst at 190 °C and 5.5 MPa. It was concluded that low conversion was achieved over the catalysts which were treated at low temperature (190 °C). Hexagonal morphology was shown by bulk nickel phosphide catalyst. After annealing, the sample synthesized at a pH of 9 predominantly showed metallic nickel diffraction peaks, but the sample produced at a higher pH value (pH 12) was found to be pure amorphous metallic nickel as determined by XRD. When the pH was reduced to 7, the comparatively strong diffraction peaks of Ni_3P were seen. All diffraction peaks of the annealed sample may be assigned to the Ni_3P phase when the pH value is 5. The influence of annealing temperature is also demonstrated. More substantial diffraction peaks and larger particle sizes resulted in a higher annealing temperature (600 °C), resulting in a lower dispersion degree, which is usually undesirable for catalysts. It is discovered that Ni_3P has a hexagonal prism shape, and its length-to-diameter ratio is 2 to 1 [141].

Zhang et al. studied macro-mesoporous carbon (MMCs) encapsulated in Ni nanoparticles catalysts synthesized by dual-templating technique for glycerol hydrogenolysis to 1,2-PDO. On hierarchical catalysts, the glycerol conversion of 95.5% was achieved along with 77.1% selectivity of 1,2-PDO over Ni/MMC-6 catalyst at 210 °C and 4 MPa. Ni supported on multiporous carbon was highly active, stable, and selective catalysts for hydrogenolysis of glycerol to PDO. These catalysts' performance was attributed to their

large surface area and pore volume proposed to reduce mass transfer limitation in the system. The total surface area and pore volume of the Ni/MMC-X materials were found to be much greater than those of the Ni/C micro and Ni/CNT (Ni modified carbon nanotubes) materials [154].

Chimentão et al. investigated zinc-supported Cu and Ni catalysts for glycerol hydrogenolysis. 100% transformation of glycerol was achieved over Ni/ZnAl catalyst. 55% and 49% selectivity of hydroxyacetone and 29% and 26% yield of hydroxy acetone were achieved over Cu/ZnAl and Cu/ZnO catalyst simultaneously at 300 °C. Ni promoted catalysts that formed methane, and Cu promoted catalysts that acetol formation. The thermodynamically stable phase of zinc oxide at ambient conditions is zincite, which crystallizes in the hexagonal wurtzite structural type. It was mentioned that the acidity of ZnAl and ZnO promoted activity. Adsorption and acidity played a vital role in the transformation of glycerol [155]. The catalyst has both acidic as well as basic sites. The basic sites' influence must also be considered. The mechanism of glycerol dehydration for acetol formation over basic sites was proposed [95]. The reaction mechanism proposed over basic sites began with the dehydrogenation step rather than the dehydration step [156] (Figure 7).

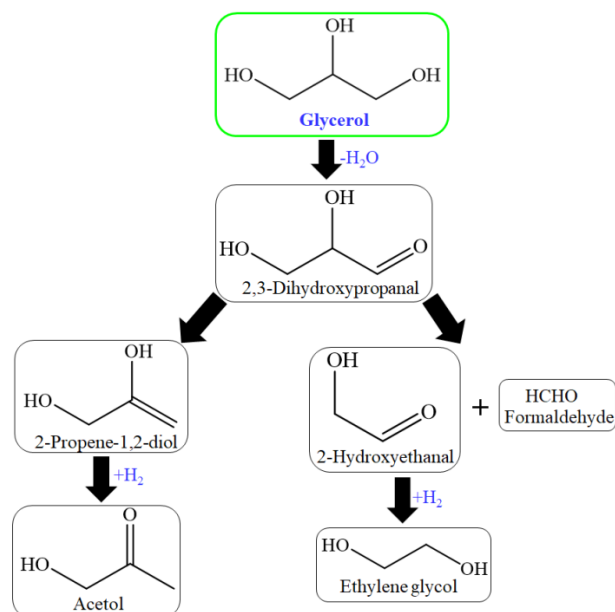


Figure 7. Reaction process over basic sites of HZSM-5 catalyst for glycerol conversion.

In this, 2,3-dihydroxypropanal, through dehydration and hydrogenation produced acetol and/or through the retro-aldol reaction of formaldehyde and 2-hydroxyethanal (hydroxyacetaldehyde) to produce ethylene glycol through hydrogenation [93,95,156]. The glycerol hydrogenolysis mechanism is suggested in two steps for propylene glycol (1,2-PDO, 1,3-PDO) production: dehydration and hydrogenation. The mechanism of glycerol hydrogenolysis involves dehydration first and then hydrogenation. The different dehydration intermediates of glycerol correspond to propylene glycol through hydrogenation. The tautomeric equilibrium is indicated as a double-arrow between the dehydration intermediates (Figure 8) [157,158].

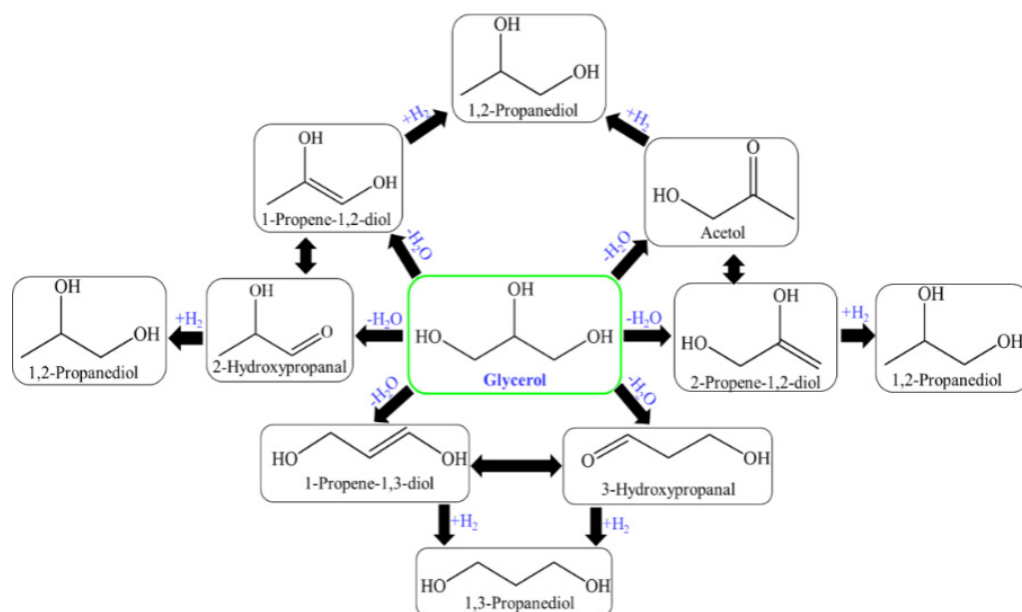


Figure 8. Glycerol hydrogenolysis for the production of 1,2-PDO and 1,3-PDO through different reaction intermediates.

4.2. Copper Catalysts for Glycerol Hydrogenolysis

Bimetallic Ru–Cu nanoparticles supported over the series of TiO₂ catalysts prepared from the impregnation method for hydrogenolysis of glycerol for 1,2-PDO production was studied [142]. 53.9% glycerol conversion and 93.2% 1,2-PDO selectivity were achieved of 2.5Ru-2.5Cu/TiO₂ catalyst at 200 °C and 2.5 MPa. The best performance was shown by 2.5Ru-2.5Cu/TiO₂ catalyst and concluded that the addition of Ru-Cu-based catalyst enhanced 1,2-PDO selectivity. Copper-supported activated carbon through the impregnation method for glycerol production of 1,2-PDO [159]. The maximum glycerol transformation of 23%, along with 20% 1,2-PDO selectivity, was achieved over copper (Cu) supported on activated carbon treated at 750 °C (Cu/CGran(750)) at 220 °C and 5 MPa. The interaction of Cu species with carbon support was minimized at high temperatures, leading to large Cu particles. Novel bi-functional Cu–Mg/SiO₂ catalyst through chemisorptions–hydrolysis technique for production of 1,2-PDO from hydrogenolysis of glycerol and 89.5% transformation of glycerol, as well as 92.1% selectivity of 1,2-PDO achieved over Cu_{0.1}-Mg_{0.2}, supported SiO catalyst at 210 °C and 4 bar [160]. The result revealed that Cu species were enough active sites for maximum activity, the addition of copper reduced the Lewis acid sites and enhanced the Bronsted acid sites. Shan et al. investigated Cu/SBA-15 catalyst through a simply grinding technique and impregnation method for 1,2-PDO production from hydrogenolysis of glycerol. A 90.3% transformation of glycerol along with 97.3% 1,2-PDO selectivity was achieved at 10% Cu/SBA-15 prepared through grinding method at 230 °C and 4 MPa. Cu/SBA-15 catalysts with large surface areas showed excellent stability as well as activity in the hydrogenolysis reaction of glycerol [161].

4.3. Platinum Catalysts for Glycerol Hydrogenolysis

Feng et al. studied tungsten (W) and aluminum (Al) doped into SBA-15 through one-step technology in the acidic medium for glycerol hydrogenolysis for 1,3-PDO production. Diffraction peaks were detected clearly after the metal ions were incorporated into the SBA-15 framework, suggesting that the SBA-15 mesoporous structure was well conserved after the direct synthesis [162]. The glycerol transformation was 66%, and 50% 1,3-PDO selectivity was achieved over Pt supported (W+Al) modified SBA-15 catalyst at 160 °C and 6 MPa. Niu et al. investigated WO_x-supported Pt catalysts prepared through hydrothermally and impregnation method for hydrogenolysis of glycerol to 1,3-PDO [163]. Pt doped over HWO₃ catalyst produced 63.4% glycerol transformation and 43.1% 1,3-

PDO selectivity at 5 MPa and 160 °C. The enhancement in performance showed the Pt nanoparticle dispersion, the high acidic nature, and the interaction of HWO₃. The tungsten modification effect on phosphate-supported zirconia Pt catalyst for hydrogenolysis to produce 1-propanol [164].

Wang et al. achieved glycerol conversion 100% and 81% 1-Propanol yield was achieved at Pt/7WO_x-ZrP catalyst at 270 °C and 2 MPa. It was concluded that the modification of ZrPWO_x increased the catalyst's total acidity, which was beneficial for glycerol conversion and also enhanced Pt nanoparticles dispersion. The addition of WO_x mainly improved Lewis acid sites, while Brønsted acid sites remained the same. Various supported, as well as unsupported, Pt-W-based catalysts to produce 1,3-PDO from the hydrogenolysis of glycerol. Among all, Pt-WO_x doped Al₂O₃ provided the best activity and selectivity and showed strong dispersion of Pt over WO_x which promoted strong Bronsted acidic sites [165].

4.4. Iron Catalysts for Glycerol Hydrogenolysis

Heterogeneous iron-containing nanocrystals for the hydrogenolysis of glycerol and mentioned that the incorporation of Fe metal positively affected selectivity and activity of catalysts for glycerol hydrogenolysis towards 1,2-PDO [153]. The recent achievements in Fe-based heterogeneous catalysts in the hydrogenolysis and hydrogenation process are outlined in this review. Lopez et al. studied hydrotalcite-supported transition metals (Fe, Zn, Ni, and Cu) prepared by the coprecipitation technique for hydrogenolysis of glycerol for 1,3-PDO production and 89.7% glycerol transformation along with 82.6% yield and 92% selectivity of 1,2-PDO was achieved over 15 wt.% Cu supported on hydrotalcite (HDTs-Cu) catalyst at 3.4 MPa and 200 °C. The highest activity and 1,2-PDO selectivity were achieved over copper-modified catalysts even with 62% purity of crude glycerol employed.

By comparing these peaks, it was discovered that when the metals iron, nickel, copper, and zinc were replaced in the environment with laminar octahedral brucite coordination, the intensity of the characteristic peak (003) increased, indicating an increase in structural integrity by assuming trilaminar rhombohedral layer stacking. When the surface properties of several HDT-type catalytic materials were characterized, an area drop was seen when the cation ionic radius (ionic radius, Fe, Ni, Cu, and Zn) increased. However, HDT-Ni was an exception because its area value was lower than those achieved with materials containing Cu and Zn. Ni has a shorter ionic radius than Cu and Zn; therefore, it was hypothesized that the catalyst incorporating Ni would have a larger surface area. This can likely be linked to the material's synthesis or maturation [166].

4.5. Cerium Catalysts for Glycerol Hydrogenolysis

Cerium (Ce) promoted Cu/Mg catalyst through coprecipitation method for production 1,2-PDO through hydrogenolysis of glycerol. The activity of catalysts for glycerol hydrogenolysis was achieved in order: Cu/Mg < Cu/Ce1/Mg < Cu/Ce5/Mg < Cu/Ce3/Mg. The markable point was that CeO₂ and Cu/Mg with atomic ratio = 3/5 catalyst might be used several times for hydrogenolysis reaction of glycerol without reducing activity. It is worth noting that the Cu/Ce1/Mg and Cu/Ce3/Mg samples revealed varied XRD peaks corresponding to CuO phases, but the metallic Cu phase showed no XRD peaks. When compared to pure CeO₂, the CeO₂ diffraction peaks of Ce-promoted Cu/Mg materials were moved to the higher angle side. This odd observation could be due to the interaction between CeO₂ and Cu/Mg samples [139].

4.6. Silver Catalysts for Glycerol Hydrogenolysis

A series of silver-modified catalysts for hydrogenolysis of glycerol produced 1,2-PDO; 78.8% conversion and 54.2% selectivity of 1,2-PDO over Raney-Ni₃₄Ag catalyst at 210 °C and 4 MPa. Ag modified catalyst presented better activity and enhanced C₃ product selectivity contrasted with unmodified Raney nickel (R-Ni) catalyst. At low and high magnification, SEM pictures of the R-Ni-based catalysts revealed a prominent porosity

zone, indicating that fresh R-Ni is a high-surface-area catalyst made up of reduced Ni particles. R-Ni had a BET surface area of $21.1 \text{ m}^2\text{gcat}^{-1}$ after drying and passivation, which increased to $42.4 \text{ m}^2\text{gcat}^{-1}$ when a modest amount of Ag was added to R-Ni and reduced significantly when more Ag was added [140].

Summary of some more reported literature related to glycerol reforming over heterogeneous catalysts to produce propylene glycol (1,2-PDO, 1,3-PDO), and ethylene glycol is represented in Tables 4 and 5.

Table 4. Glycerol hydrogenolysis over various catalytic systems for 1,2-PDO production.

S. No.	Catalysts	Reaction Conditions/Reactor	X (%)	S (%)	Y (%)	References
1	Nickel phosphide	T = 463 K P = 5.5 MPa (Autoclave reactor)	5.4	95.3	5.15	[141]
2	2.5Ru-2.5Cu/TiO ₂ (Impregnation method)	T = 473 K P = 2.5 MPa Cat. Wt. = 0.6 g	53.9	93.2	50.2	[142]
3	Cu _{0.1} -Mg _{0.2} supported SiO ₂ (Chemisorption–hydrolysis method)	T = 210 °C P = 45 bar (Autoclave reactor)	89.5	92.1	81.2	[160]
4	10% Cu/SBA-15 (Grinding and Impregnation method)	T = 503 K P = 4 MPa	90.3	97.3	87.9	[161]
5	hydrotalcite supported Fe, Zn, Ni, and Cu (Coprecipitation method)	T = 200 °C P = 3.4 MPa	92	89.8	82.6	[166]
6	Ni–Cu/Al ₂ O ₃ (Sol–gel method)	T = 723 K P = 1 bar (Autoclave reactor)	33.5	85.9	28.8	[167]
7	Raney Ni	T = 230 °C P = 40 bar (Autoclave reactor)	80	54	43.2	[168]
8	Cu over Al ₂ O ₃ , ZnO and Cr ₂ O ₃	T = 190 °C P = 1 atm (Fixed bed reactor)	100	96.2	96.2	[169]
9	Cu over boehmite (Chemical reduction method)	T = 473 K P = 4 MPa Cat. Wt. = 0.8 g (Autoclave reactor)	77.5	92.5	71.2	[170]
10	B ₂ O ₃ on Cu/SiO ₂ (Precipitation–gel method)	T = 200 °C P = 5 MPa WHSV = 0.075 h ^{−1} (Fixed bed reactor)	98.5	96.7	95.2	[171]
11	Pt, Pd and Ni/Fe ₃ O ₄ (Impregnation method)	T = 493 K P = 25–50 bar Cat. Wt. = 0.5 g (Fixed bed reactor)	81	79	70	[172]
12	Alumina supported bimetallic Pt–Fe (Impregnation method)	T = 513 K P = 20 bar Cat. Wt. = 0.5 g (Batch reactor)	86.2	58.2	50.2	[173]

Table 4. Cont.

S. No.	Catalysts	Reaction Conditions/Reactor	X (%)	S (%)	Y (%)	References
13	Fe ₂ O ₃ at CuMgAl	T = 190 °C P = 2 MPa	77.8	99	77	[174]
14	Ce promoted Ni/SBA-15 (Incipient method)	T = 473 K P = 2.4 MPa Cat. Wt. = 0.6 g (Autoclave Parr reactor)	50	28	14	[175]
15	Ni/Ce–Mg (Precipitation and impregnation method)	T = 215–245 °C P = 4.1–6.9 MPa Cat. Wt. = 5.0 g (Batch reactor)	80.47	74.4	59.9	[176]
16	Ni–Co bimetallic supported on γ -Al ₂ O ₃ (Impregnation method)	T = 220 °C P = 6 MPa Cat. Wt. = 2.0 g (Autoclave reactor)	63.5	60.4	38.4	[177]
17	Ni–Ag/ γ -Al ₂ O ₃ (co-impregnation method)	T = 180–260 °C P = 1 atm WHSV = 2.01 h ⁻¹ (Fixed bed reactor)	80	58	46.4	[178]
18	Ag/Al ₂ O ₃ (Impregnation method)	T = 400–500 °C P = 2.1 MPa (Batch reactor)	46	96	44.2	[179]
19	Ag–OMS-2 (Precipitation method)	T = 200 °C P = 50 atm Cat. Wt. = 28.0 g (Fixed bed reactor)	70	90	63	[180]

X = Conversion, S = Selectivity, Y = Yield.

Table 5. Glycerol hydrogenolysis over various catalytic systems for producing 1,3-PDO, propylene glycol, and ethylene glycol.

S. No.	Product	Catalysts	Reaction Conditions/Reactor	X (%)	S (%)	Y (%)	References
1	1,3-PDO	Pt–sulphated zirconia	T = 170 °C P = 7.3 MPa	66.5	83.6	55.6	[181]
2	1,3-PDO	Pt–WO ₃ on Al-based supports and Ir–ReO _x /SiO ₂ (Impregnation method)	T = 403 K P = 4 MPa	84.5	26	30	[83]
3	1,3-PDO	Pt/WO ₃ /ZrO ₂ (Impregnation method)	T = 110–140 °C P = 2–5 MPa (Fixed bed reactor)	70.2	45.6	32	[182]
4	Ethylene glycol	Pd–Ni bimetallic (Co-precipitation method)	T = 493 K P = 6 MPa (Autoclave reactor)	89	22	19.58	[183]
5	Propylene glycol	Cu–Ni (Impregnation method)	T = 250 °C P = 40 bar WHSV = 2.5 h ⁻¹ (Fixed bed reactor)	90	77.8	70	[184]
6	Propylene glycol	Cu/HMS, (Ru–Cu)/SiO ₂ , (Impregnation method)	T = 240 °C P = 8 MPa (Fixed bed reactor)	100	91	91	[185]

Table 5. Cont.

S. No.	Product	Catalysts	Reaction Conditions/Reactor	X (%)	S (%)	Y (%)	References
7	Propylene glycol	Al, Ba and Zn promoter in copper chromite	T = 493 K P = 5 MPa Cat. Wt. = 1 g (Fixed bed reactor)	34	90	30.6	[186]

X = Conversion, S = Selectivity, Y = Yield.

5. Conclusions

The knowledge of various catalysts, such as nickel, platinum, ruthenium, copper, cadmium, zeolite, titanium, alumina, iron, cerium, silver, and rhodium, steam reforming process, dehydration process, and hydrogenolysis process of glycerol was reviewed and cataloged. Numerous researchers have described various ways of converting glycerol into value-added products, such as hydrogen, acetol, acrolein, ethylene glycol, propylene glycol (1,2-propanediol, 1,3-propanediol), etc., via several reactions under different reaction conditions. These chemical compounds have a clear monetary value and can help the biodiesel industry.

Many research efforts are ongoing to overcome challenges and explore new frontiers to search for new products. Those challenges involve the selection of catalyst for some products and reaction conditions, severe difficulty in separating the catalyst from desired products, and low yields of the products with long catalytic reaction runs. Today, researchers and engineers are exploring new technologies, highly novel and tolerant catalysts, improving reactor systems and activation methods, and coordinating the chemical and biological catalysts to improve the weaknesses involved with each catalyst. The modern improvement in technology and economical use of crude glycerol for value-added product formulation clearly demonstrate that crude glycerol may play a critical part in the bio-refining industry's fulfillment.

Author Contributions: Writing—original draft preparation, N.T. and R.P.; data curation, A.P., P.B., and P.C.; formal analysis, R.R., N.M., R.G., A.B.R., and A.M.A.; original draft preparation, supervision and editing, R.B., V.P., and N.A.-Q.; funding acquisition N.A.-Q. All authors have read and agreed to the published version of the manuscript.

Funding: This work was supported by Qatar University through a National Capacity Building Program Grant (NCBP), [QUCP-CAM-2022-463]. Statements made herein are solely the responsibility of the authors.

Data Availability Statement: Not applicable.

Conflicts of Interest: The authors declare no conflict of interest.

References

- Balat, H.; Kırtay, E. Hydrogen from biomass Present scenario and future prospects. *Int. J. Hydrogen Energy* **2010**, *35*, 7416–7426. [[CrossRef](#)]
- Savage, N. Fuel options: The ideal biofuel. *Nature* **2011**, *479*, S9–S11. [[CrossRef](#)] [[PubMed](#)]
- Tollefson, J. Risky energy research faces uncertain future. *Nature* **2011**, *471*, 145–146. [[CrossRef](#)] [[PubMed](#)]
- Gielen, D.; Boshell, F.; Saygin, D.; Morgan, D.B.; Wagner, N.; Gorini, R. The role of renewable energy in the global energy transformation. *Energy Strategy Rev.* **2019**, *24*, 38–50. [[CrossRef](#)]
- Kondratenko, E.V.; Mul, G.; Baltrusaitis, J.; Larrazabal, G.O.; Pérez-Ramírez, J. Status and perspectives of CO₂ conversion into fuels and chemicals by catalytic, photocatalytic and electrocatalytic processes. *Energy Environ. Sci.* **2013**, *6*, 3112–3135. [[CrossRef](#)]
- Aresta, M.; Angelini, A.D.A. Catalysis for the Valorization of Exhaust Carbon: From CO₂ to Chemicals, Materials, and Fuels. Technological Use of CO₂. *Chem. Rev.* **2014**, *114*, 1709–1742. [[CrossRef](#)]
- Kumar, A.; Jones, D.D.; Hanna, M.A. Thermochemical Biomass Gasification: A Review of the Current Status of the Technology. *Energies* **2009**, *2*, 556–581. [[CrossRef](#)]
- Shirazi, M.A.; Kargari, A.; Tabatabaei, M.; Mostafaeid, B.; Akiaie, M.; Barkhi, M.; Shirazi, M.J.A. Acceleration of biodiesel–glycerol decantation through NaCl-assisted gravitational settling: A strategy to economize biodiesel production. *Bioresour. Technol.* **2013**, *134*, 401–406. [[CrossRef](#)]

9. Demirbas, A. Biofuels sources, biofuel policy, biofuel economy and global biofuel projections. *Energy Convers. Manag.* **2008**, *49*, 2106–2116. [CrossRef]
10. Ramyakrishna, P.; Raveendra, G.; Rajender, B.; Vijayanand, P.; Ma, J. Recent advances in biomass-derived platform chemicals to valeric acid synthesis. *New. J. Chem.* **2022**, *46*, 5907–5921.
11. Muraza, O. Peculiarities of Glycerol Conversion to Chemicals Over Zeolite-Based Catalysts. *Front. Chem.* **2019**, *7*, 233. [CrossRef] [PubMed]
12. Papageridis, K.N.; Siakavelas, G.; Charisiou, N.D.; Avraam, D.G. Comparative study of Ni, Co, Cu supported on γ -alumina catalysts for hydrogen production via the glycerol steam reforming reaction. *Fuel Process. Technol.* **2016**, *152*, 156–179. [CrossRef]
13. Silva, J.M.; Soria, M.A.; Madeira, L.M. Challenges and strategies for optimization of glycerol steam reforming process. *Renew. Sustain. Energy Rev.* **2015**, *42*, 1187–1213. [CrossRef]
14. Roberto, M.M.; Luis, K.C.; Sanaiotte, P.R.; Otávio, B.M.; Cesar, A.d.S. Glycerol from biodiesel production: Technological paths for sustainability. *Renew. Sustain. Energy Rev.* **2018**, *88*, 109–122.
15. Reangchim, P.; Daorattanachai, P.; Laosiripojana, N. Conversion of glycerol waste from biodiesel plant to high-value product. *J. Sustain. Energy Environ.* **2019**, *10*, 41–44.
16. Nda-Umar, U.I.; Ramli, I.; Taufiq-Yap, Y.H.; Muhamad, E.N. An overview of recent research in the conversion of glycerol into biofuels, fuel additives and other bio-based chemicals. *Catalysts* **2019**, *9*, 15. [CrossRef]
17. Semkiv, M.V.; Ruchala, J.; Dmytruk, K.V.; Sibirny, A.A. 100 Years Later, What Is New in Glycerol Bioproduction? *Trend Biotechnol.* **2020**, *38*, 907–916. [CrossRef]
18. Tan, H.W.; Aziz, A.R.A.; Aroua, M.K. Glycerol production and its applications as a raw material: A review. *Renew. Sustain. Energy Rev.* **2013**, *27*, 118–127. [CrossRef]
19. Len, C.; Luque, R. Continuous flow transformations of glycerol to valuable products: An overview. *Sustain. Chem. Process.* **2014**, *2*, 1. [CrossRef]
20. Bos, H.L.; Harmsen, P.F.H.; Annevelink, E. Background Information and Biorefinery Status, Potential and Sustainability: Task 2.1.2 Market and Consumers. *Carbohydrates*. 2010, pp. 1–28. Available online: <https://library.wur.nl/WebQuery/wurpubs/reports/399310> (accessed on 5 May 2022).
21. Nanda, R.M.; Zhang, Y.; Yuan, Z.; Qin, W.; Ghaziaskar, H.S.; Xu, C. Catalytic conversion of glycerol for sustainable production of solketal as a fuel additive: A review. *Renew. Sustain. Energy Rev.* **2016**, *56*, 1022–1031. [CrossRef]
22. Rahmat, N.; Abdullah, A.Z.; Mohamed, A.R. Recent progress on innovative and potential technologies for glycerol transformation into fuel additives: A critical review. *Renew. Sustain. Energy Rev.* **2010**, *372*, 224–238. [CrossRef]
23. Martin, M.; Richter, A. Oligomerization of glycerol—A critical review. *Eur. J. Lipid Sci. Technol.* **2011**, *113*, 100–117. [CrossRef]
24. Razali, N.; Abdullah, A.Z. Production of lactic acid from glycerol via chemical conversion using solid catalyst: A review. *Appl. Catal. A Gen.* **2017**, *543*, 234–246. [CrossRef]
25. Teng, W.K.; Ngoh, G.C.; Yusoff, R.; Aroua, M.K. A review on the performance of glycerol carbonate production via catalytic transesterification: Effects of influencing parameters. *Energy Convers. Manag.* **2014**, *88*, 484–497. [CrossRef]
26. Checa, M.; Nogales-Delgado, S.; Montes, V.; Encinar, J.M. Recent Advances in Glycerol Catalytic Valorization: A Review. *Catalysts* **2020**, *10*, 1279. [CrossRef]
27. Zakaria, Z.Y.; Amin, N.A.S.; Linnekoski, J. A perspective on catalytic conversion of glycerol to olefins. *Biomass Bioenergy* **2013**, *55*, 370–385. [CrossRef]
28. Anitha, M.; Kamarudina, S.K.; Kofli, N.T. The potential of glycerol as a value-added commodity. *Chem. Eng. J.* **2016**, *295*, 119–130. [CrossRef]
29. Wu, K.; Dou, B.; Zhang, H.; Liu, D.; Chen, H.; Xu, Y. Aqueous phase reforming of biodiesel byproduct glycerol over mesoporous Ni-Cu/CeO₂ for renewable hydrogen production. *Fuel* **2022**, *308*, 122014. [CrossRef]
30. Liu, D.; Dou, B.; Zhang, H.; Zhao, L.; Wu, K.; Zeng, P.; Chen, H.; Xu, Y. Comparison of gelatinous and calcined magnesia supported Ni or/and Co-based catalysts for aqueous phase reforming of glycerol. *Renew. Energy* **2022**, *186*, 656–666. [CrossRef]
31. Zoppi, G.; Pipitone, G.; Pirone, R.; Bensaid, S. Aqueous phase reforming process for the valorization of wastewater streams: Application to different industrial scenarios. *Catal. Today* **2022**, *387*, 224–236. [CrossRef]
32. Su, H.; Yan, M.; Wang, S. Recent advances in supercritical water gasification of biowaste catalyzed by transition metal-based catalysts for hydrogen production. *Renew. Sustain. Energy Rev.* **2022**, *154*, 111831. [CrossRef]
33. Dou, B.; Zhao, L.; Zhang, H.; Wu, K.; Zhang, H. Renewable hydrogen production from chemical looping steam reforming of biodiesel byproduct glycerol by mesoporous oxygen carriers. *Chem. Eng. J.* **2021**, *416*, 127612. [CrossRef]
34. Felseghi, R.A.; Carcadea, E.; Raboaca, M.S.; Trufin, C.N.; Filote, C. Hydrogen Fuel Cell Technology for the Sustainable Future of Stationary Applications. *Energies* **2019**, *12*, 4593. [CrossRef]
35. Markocic, E.; Kramberger, B.; Van Bennekom, J.G.; Heeres, H.J.; Vos, J.; Knez, Z. Glycerol reforming in supercritical water; a short review. *Renew. Sustain. Energy Rev.* **2013**, *23*, 40–48. [CrossRef]
36. Al-Salihi, S.; Abrokwhah, R.; Dade, W.; Deshmane, V.; Hossain, T.; Kuila, D. Renewable hydrogen from glycerol steam reforming using Co-Ni-MgO based SBA-15 nanocatalysts. *Int. J. Hydrogen Energy* **2020**, *45*, 14183–14198. [CrossRef]
37. El Doukkali, M.; Iriondo, A.; Cambra, J.F.; Gandarias, I.; Jalowiecki-Duhamel, L.; Dumeignil, F.; Arias, P.L. Deactivation study of the Pt and/or Ni-based -Al₂O₃ catalysts used in the aqueous phase reforming of glycerol for H₂ production. *Appl. Catal. A Gen.* **2014**, *472*, 80–91. [CrossRef]

38. Pompeo, F.; Santori, G.F.; Nichio, N.N. Hydrogen production by glycerol steam reforming with Pt/SiO₂ and Ni/SiO₂ catalysts. *Catal. Today* **2011**, *172*, 183–188. [[CrossRef](#)]
39. Huang, X.; Dang, C.; Yu, H.; Wang, H.; Peng, F. Morphology Effect of Ir/La₂O₂CO₃ Nanorods with Selectively Exposed {110} Facets in Catalytic Steam Reforming of Glycerol. *ACS Catal.* **2015**, *5*, 1155–1163. [[CrossRef](#)]
40. Kim, J.; Kim, J.; Lee, D. Glycerol steam reforming on Ru catalysts supported on core-shell metal–ceramic microcomposites developed by a microwave-induced hydrothermal method. *Appl. Catal. A Gen.* **2015**, *449*, 197–204. [[CrossRef](#)]
41. Sundari, R.; Vaidya, P.D. Reaction Kinetics of Glycerol Steam Reforming Using a Ru/Al₂O₃ Catalyst. *Energy Fuels* **2012**, *26*, 4195–4204. [[CrossRef](#)]
42. Baca, S.; Sayb, Z.; Kocak, Y.; Ercanb, K.; Harfouched, M.; Ozensoy, E.; Avci, A.K. Exceptionally active and stable catalysts for CO₂ reforming of glycerol to syngas. *Appl. Catal. B Environ.* **2019**, *256*, 117808. [[CrossRef](#)]
43. Vaidya, P.D.; Rodrigues, A.E. Glycerol Reforming for Hydrogen Production: A Review. *Chem. Eng. Technol.* **2009**, *32*, 1463–1469. [[CrossRef](#)]
44. Martinez, L.M.T.; Araque, M.; Vargas, J.C.; Roger, A.C. Effect of Ce/Zr ratio in CeZr-CoRh catalysts on the hydrogen production by glycerol steam reforming. *Appl. Catal. A Gen.* **2013**, *132–133*, 499–510. [[CrossRef](#)]
45. Lee, J.; Doohwan, K. Synthesis and Properties of Core–Shell Metal–Ceramic Microstructures and their Application as Heterogeneous Catalysts. *ChemCatChem* **2014**, *6*, 2642–2647.
46. Delparish, A.; Koc, S.; Caglayan, B.S.; Avc, A.K. Oxidative steam reforming of glycerol to synthesis gas in a microchannel reactor. *Catal. Today* **2019**, *323*, 200–208. [[CrossRef](#)]
47. Danga, C.; Wu, S.; Yang, G.; Cao, Y.; Wang, H.; Peng, F.; Yu, H. Syngas production by dry reforming of the mixture of glycerol and ethanol with CaCO₃. *J. Energy Chem.* **2020**, *43*, 90–97. [[CrossRef](#)]
48. Rezendea, S.M.D.; Franchini, C.A.; Dieuzeide, M.L.; de Farias, A.M.D.; Amadeo, N.; Fraga, M.A. Glycerol steam reforming over layered double hydroxide-supported Pt catalysts. *Chem. Eng. J.* **2015**, *272*, 108–118. [[CrossRef](#)]
49. Charisiou, N.D.; Italiano, C.; Pino, L.; Sebastian, V.; Vita, A.; Goula, M.A. Hydrogen production via steam reforming of glycerol over Rh/ γ -Al₂O₃ catalysts modified with CeO₂, MgO or La₂O₃. *Renew. Energy* **2020**, *162*, 908–925. [[CrossRef](#)]
50. Wu, G.; Zhang, C.; Li, S.; Han, Z.; Wang, T.; Ma, X.; Gong, J. Hydrogen Production via Glycerol Steam Reforming over Ni/Al₂O₃: Influence of Nickel Precursors. *ACS Sustain. Chem. Eng.* **2013**, *1*, 1052–1062. [[CrossRef](#)]
51. Sánchez, N.; Encinar, J.M.; González, J.F. Sorption Enhanced Steam Reforming of Glycerol: Use of La-Modified Ni/Al₂O₃ as Catalyst. *Ind. Eng. Chem. Res.* **2016**, *55*, 3736–3741. [[CrossRef](#)]
52. Ruppert, R.A.M.; Niewiadomski, M.; Grams, J.; Kwapiński, W. Optimization of Ni/ZrO₂ catalytic performance in thermochemical cellulose conversion for enhanced hydrogen production. *Appl. Catal. B Environ.* **2014**, *145*, 85–90.
53. Yan, Z.; Liu, S.; Zhang, Y.; Wang, T.; Luo, S.; Chu, W.; Jing, F. The role of Zr in NiZrAl oxides catalyst and the evaluation on steam reforming of glycerol for hydrogen product. *Catal. Today* **2019**, *319*, 229–238. [[CrossRef](#)]
54. Charisiou, C.N.D.; Siakavelas, G.; Tzounis, L.; Dou, B.; Sebastian, V.; Hinder, S.J.; Baker, M.A.; Polychronopoulou, K.; Goula, M.A. Ni/Y₂O₃–ZrO₂ catalyst for hydrogen production through the glycerol steam reforming reaction. *Int. J. Hydrogen Energy* **2020**, *45*, 10442–10460. [[CrossRef](#)]
55. Xiong, Y.; Wang, B.; Yan, J.; Hong, J.; Wang, L.; Zhang, Y.; Li, J.; Jing, F.; Chu, W. Plasma assisted preparation of nickel-based catalysts supported on CeO₂ with different morphologies for hydrogen production by glycerol steam reforming. *Powder Technol.* **2019**, *345*, 324–332. [[CrossRef](#)]
56. Yancheshmeh, M.S.; Alizadeh, O.S.; Aissaoui, M.; Iliuta, M.C. A novel synthesis of NiAl₂O₄ spinel from a Ni–Al mixed-metal alkoxide as a highly efficient catalyst for hydrogen production by glycerol steam reforming. *Appl. Catal. B Environ.* **2020**, *265*, 118535. [[CrossRef](#)]
57. Feng, P.; Huang, K.; Xu, Q.; Qi, W.; Xin, S.; Wei, T.; Liao, L.; Yan, Y. Ni supported on the CaO modified attapulgite as catalysts for hydrogen production from glycerol steam reforming. *Int. J. Hydrogen Energy* **2020**, *45*, 8223–8233. [[CrossRef](#)]
58. Veiga, S.; Faccio, R.; Romero, M.; Bussi, J. Utilization of waste crude glycerol for hydrogen production via steam reforming over Ni–La–Zr catalysts. *Biomass Bioenerg.* **2020**, *135*, 105508. [[CrossRef](#)]
59. Ghungrud, S.A.; Vaidya, P.D. Sorption-enhanced reaction process for glycerol-to-hydrogen conversion over cobalt catalyst supported on promoted hydrotalcites. *Int. J. Hydrogen Energy* **2020**, *45*, 9440–9450. [[CrossRef](#)]
60. Zhou, H.; Liu, S.; Jing, F.; Luo, S.Z.; Shen, J.; Pang, Y.; Chu, W. Synergetic Bimetallic NiCo/CNT Catalyst for Hydrogen Production by Glycerol Steam Reforming: Effects of Metal Species Distribution. *Ind. Eng. Chem. Res.* **2020**, *59*, 17259–17268. [[CrossRef](#)]
61. Seretis, A.; Tsiakaras, P. Aqueous phase reforming (APR) of glycerol over platinum supported on Al₂O₃ catalyst. *Renew. Energy* **2016**, *85*, 1116–1126. [[CrossRef](#)]
62. Callison, J.; Subramanian, N.D.; Rogers, S.M.; Chutia, A.; Gianoliod, D.; Catlow, C.R.A.; Wells, P.P.; Dimitratos, N. Directed aqueous-phase reforming of glycerol through tailored platinum nanoparticles. *Appl. Catal. B Environ.* **2018**, *238*, 618–628. [[CrossRef](#)]
63. Touri, A.E.; Taghizadeh, M. Hydrogen Production via Glycerol Reforming over Pt/SiO₂ Nanocatalyst in a Spiral-Shaped Microchannel Reactor. *Int. J. Chem. React.* **2016**, *14*, 1059–1068. [[CrossRef](#)]
64. Ciftci, A.; Peng, B.; Jentys, A.; Lercher, J.A.; Hensen, E.J.M. Support effects in the aqueous phase reforming of glycerol over supported platinum catalysts. *Appl. Catal. A Gen.* **2012**, *431–432*, 113–119. [[CrossRef](#)]

65. Pompeo, F.; Santori, G.; Nichio, N.N. Hydrogen and/or syngas from steam reforming of glycerol. Study of platinum catalysts. *Int. J. Hydrogen Energy* **2010**, *35*, 8912–8920. [[CrossRef](#)]
66. Lehnert, K.; Claus, P. Influence of Pt particle size and support type on the aqueous-phase reforming of glycerol. *Catal. Commun.* **2008**, *9*, 2543–2546. [[CrossRef](#)]
67. King, D.L.; Zhang, L.; Xia, G.; Karim, A.M.; Heldebrant, D.J.; Wang, X.; Peterson, T.; Wang, Y. Aqueous phase reforming of glycerol for hydrogen production over Pt–Re supported on carbon. *Appl. Catal. B Environ.* **2010**, *99*, 206–213. [[CrossRef](#)]
68. Demsash, H.D.; Kondamudi, K.V.K.; Upadhyayula, S.; Mohan, R. Ruthenium doped nickel-alumina-ceria catalyst in glycerol steam reforming. *Fuel Process. Technol.* **2018**, *169*, 150–156. [[CrossRef](#)]
69. Dahdah, E.; Aouad, S.; Gennequin, C.J.E.; Nsouli, B.; Aboukais, A.; Abi-Aad, E. Glycerol steam reforming over Ru–Mg–Al hydrotalcite-derived mixed oxides: Role of the preparation method in catalytic activity. *Int. J. Hydrogen Energy* **2018**, *43*, 19864–19872. [[CrossRef](#)]
70. Kousi, K.; Kondarides, D.I.; Verykios, X.E.; Papadopoulou, C. Glycerol steam reforming over modified Ru/Al₂O₃ catalysts. *Appl. Catal. A Gen.* **2017**, *542*, 201–211. [[CrossRef](#)]
71. Gallegos-Suárez, E.; Guerrero-Ruiz, A.; Rodríguez-Ramos, I. Efficient hydrogen production from glycerol by steam reforming with carbon supported ruthenium catalysts. *Carbon* **2016**, *96*, 578–587. [[CrossRef](#)]
72. Galloa, A.; Pirovano, C.; Ferrini, P.; Marelli, M.; Psaroc, R.; Santangelo, S.; Faggio, G.; Santo, V.D. Influence of reaction parameters on the activity of ruthenium based catalysts for glycerol steam reforming. *Appl. Catal. B Environ.* **2012**, *121–122*, 40–49. [[CrossRef](#)]
73. Simonetti, D.A.; Kunkes, E.L.; Dumesic, J.A. Gas-phase conversion of glycerol to synthesis gas over carbon-supported platinum and platinum–rhenium catalysts. *J. Catal.* **2007**, *247*, 298–306. [[CrossRef](#)]
74. Bulutoglu, P.S.; Say, Z.; Bac, S.; Ozensoy, E.; Avci, A.K. Dry Reforming of Glycerol Over Rh-Based Ceria and Zirconia Catalysts: New Insights on Catalyst Activity and Stability. *Appl. Catal. A Gen.* **2018**, *564*, 157–171. [[CrossRef](#)]
75. Larimi, A.; Khorasheh, F. Renewable hydrogen production over Pt/Al₂O₃ nano-catalysts: Effect of M-promoting (M=Pd, Rh, Re, Ru, Ir, Cr). *Int. J. Hydrogen Energy* **2019**, *44*, 8243–8251. [[CrossRef](#)]
76. Oliveira, E.V.; Seixas, A.C.M.; Jordão, E. Performance of Pt and Pt–Rh Catalyst in the Hydrogen Production from Glycerol. *Can. J. Chem. Eng.* **2017**, *95*, 2018–2023. [[CrossRef](#)]
77. Chiodo, V.; Freni, S.; Galvagno, A.; Mondello, N.; Frusteri, F. Catalytic features of Rh and Ni supported catalysts in the steam reforming of glycerol to produce hydrogen. *Appl. Catal. A Gen.* **2010**, *381*, 1–7. [[CrossRef](#)]
78. Veiga, S.; Faccio, R.; Segobia, D.; Apesteguia, C.; Bussi, J. Hydrogen production by crude glycerol steam reforming over Ni/La/Ti mixed oxide catalysts. *Int. J. Hydrogen Energy* **2017**, *42*, 30525–30534. [[CrossRef](#)]
79. Suffredini, D.F.P.; Thyssen, V.V.; de Almeida, P.M.M.; Gomes, R.S.; Borges, M.C.; de Farias, A.M.D.; Assaf, E.M.; Fraga, M.A.; Brandão, S.T. Renewable hydrogen from glycerol reforming over nickel aluminate-based catalysts. *Catal. Today* **2016**, *289*, 96–104. [[CrossRef](#)]
80. Siew, K.W.; Lee, H.C.; Gimbin, J.; Chin, S.Y.; Khan, M.R.; Taufiq-Yap, Y.H.; Cheng, C.K. Syngas production from glycerol-dry (CO₂) reforming over La-promoted Ni/Al₂O₃ catalyst. *Renew. Energy* **2015**, *74*, 441–447. [[CrossRef](#)]
81. Wu, G.; Li, S.; Zhang, C.; Wang, T.; Gong, J. Glycerol steam reforming over perovskite-derived nickel-based catalysts. *Appl. Catal. B Environ.* **2014**, *144*, 277–285. [[CrossRef](#)]
82. Sanchez, E.A.; Comelli, R.A. Hydrogen production by glycerol steam-reforming over nickel and nickel-cobalt impregnated on alumina. *Int. J. Hydrogen Energy* **2014**, *39*, 8650–8655. [[CrossRef](#)]
83. Buffoni, I.N.; Pompeo, F.; Santori, G.F.; Nichio, N.N. Nickel catalysts applied in steam reforming of glycerol for hydrogen production. *Catal. Commun.* **2009**, *10*, 1656–1660. [[CrossRef](#)]
84. Aman, D.; Radwan, D.; Ebaid, M.; Mikhail, M.S.; van Steen, S.E. Comparing nickel and cobalt perovskites for steam reforming of glycerol. *Mol. Catal.* **2018**, *425*, 60–67. [[CrossRef](#)]
85. Reynoso, A.J.; Ayastuy, J.L.; Iriarte-Velasco, U.; Gutierrez-Ortiz, M.A.; Chemical Technologies for the Environmental Sustainability Group. Cobalt aluminate spinel-derived catalysts for glycerol aqueous phase reforming. *Appl. Catal. B Environ.* **2018**, *239*, 86–101. [[CrossRef](#)]
86. Dobosz, J.; Cichy, M.; Zawadzki, M.; Borowieck, T. Glycerol steam reforming over calcium hydroxyapatite supported cobalt and cobalt-cerium catalysts. *J. Energy Chem.* **2018**, *27*, 404–412. [[CrossRef](#)]
87. Carrero, A.; Vizcaino, A.J.; Calles, J.A.; García-Moreno, L. Hydrogen production through glycerol steam reforming using Co catalysts supported on SBA-15 doped with Zr, Ce and La. *J. Energy Chem.* **2016**, *26*, 42–48. [[CrossRef](#)]
88. Surendar, M.; Sagar, T.V.; Babu, B.H.; Lingaiah, B.; Rao, K.S.R.; Prasad, P.S.S. Glycerol steam reforming over La–Ce–Co mixed oxide-derived cobalt catalysts. *ACS Catal.* **2015**, *5*, 45184–45193. [[CrossRef](#)]
89. Cheng, C.K.; Foo, S.Y.; Adesina, A.A. H₂-rich synthesis gas production over Co/Al₂O₃ catalyst via glycerol steam reforming. *Catal. Commun.* **2010**, *12*, 292–298. [[CrossRef](#)]
90. Zhang, B.; Tang, X.; Li, Y.; Xu, Y.; Shen, W. Hydrogen production from steam reforming of ethanol and glycerol over ceria-supported metal catalysts. *Int. J. Hydrogen Energy* **2007**, *32*, 2367–2373. [[CrossRef](#)]
91. Groll, H.P.A.; Oakland; Hearne, G. Process of Converting a Polyhydric Alcohol to a Carbonyl Compound. U.S. Patent US2042224A, 26 May 1934.

92. Mahendran, S.; Nithya, T.; Raju, K.P.; Viswanathan, B.; Selvam, P. Dehydration of glycerol over high surface area γ -alumina supported heteropoly acid catalysts. In Proceedings of the Chemeca 2011: Engineering a Better World, Sydney Hilton Hotel, Sydney, NSW, Australia, 18–21 September 2011; Barton, A.C.T., Ed.; Engineers Australia: Redcliffe, Australia, 2011; pp. 1263–1273.
93. Katryniok, B.; Paul, S.; Belliere-Baca, V.; Rey, P.; Dumeignil, F. Glycerol dehydration to acrolein in the context of new uses of glycerol. *Green Chem.* **2010**, *12*, 2079–2098. [[CrossRef](#)]
94. Chai, S.H.; Wang, H.P.; Liang, Y.; Xu, B.Q. Sustainable production of acrolein: Investigation of solid acid–base catalysts for gas-phase dehydration of glycerol. *Green Chem.* **2007**, *9*, 1130–1136. [[CrossRef](#)]
95. Tsukuda, E.; Sato, S.; Takahashi, R.J.; Sodesawa, T. Production of acrolein from glycerol over silica-supported heteropoly acids. *Catal. Commun.* **2007**, *8*, 1349–1353. [[CrossRef](#)]
96. Corma, A.; Iborra, S.; Velty, A. Chemical Routes for the Transformation of Biomass into Chemicals. *Chem. Rev.* **2007**, *107*, 2411–2502. [[CrossRef](#)] [[PubMed](#)]
97. Alhanash, A.; Kozhevnikov, V.E.; Ivan, F.K. Gas-phase dehydration of glycerol to acrolein catalysed by caesium heteropoly salt. *Appl. Catal. A Gen.* **2010**, *378*, 11–18. [[CrossRef](#)]
98. Foo, G.S.; Wei, D.; Sholl, D.S.; Sievers, C. Role of Lewis and Brønsted Acid Sites in the Dehydration of Glycerol over Niobia. *ACS Catal.* **2014**, *4*, 3180–3192. [[CrossRef](#)]
99. Lin, X.; Lv, Y.; Qu, Y.; Zhang, G.; Xi, Y.; Phillips, D.L.; Liu, C. A combined experimental and computational study of the catalytic dehydration of glycerol on microporous zeolites: An investigation of the reaction mechanism and acrolein selectivity. *Phys. Chem. Chem. Phys.* **2013**, *15*, 20120–20133. [[CrossRef](#)]
100. Ren, X.; Zhang, F.; Sudhakar, M.; Wang, N.; Dai, J.; Liu, L. Gas-phase dehydration of glycerol to acrolein catalyzed by hybrid acid sites derived from transition metal hydrogen phosphate and meso-HZSM-5. *Catal. Today* **2019**, *332*, 20–27. [[CrossRef](#)]
101. Neves, T.M.; Fernandes, J.O.; Lião, L.M.; da Silva, E.D.; da Rosa, C.A.; Mortola, V.B. Glycerol dehydration over micro- and mesoporous ZSM-5 synthesized from a onestep method. *Microporous Mesoporous Mater.* **2019**, *275*, 244–252. [[CrossRef](#)]
102. Qureshi, B.A.; Lan, X.; Arslan, M.T.; Wang, T. Highly Active and Selective Nano H-ZSM-5 Catalyst with Short Channels along b-Axis for Glycerol Dehydration to Acrolein. *Ind. Eng. Chem. Res.* **2019**, *58*, 12611–12622. [[CrossRef](#)]
103. Yun, D.; Kim, T.Y.; Park, D.S.; Yun, Y.S.; Han, J.W.; Yi, J. A Tailored Catalyst for the Sustainable Conversion of Glycerol to Acrolein: Mechanistic Aspect of Sequential Dehydration. *ChemSusChem* **2014**, *7*, 2193–2201. [[CrossRef](#)]
104. Xie, Q.; Li, S.; Gong, R.; Zheng, G.; Wang, Y.; Xu, P.; Duan, Y.; Yu, S.; Lu, M.; Ji, W.; et al. Microwave-assisted catalytic dehydration of glycerol for sustainable production of acrolein over a microwave absorbing catalyst. *Appl. Catal. B Environ.* **2019**, *243*, 455–462. [[CrossRef](#)]
105. Shan, J.; Li, Z.; Zhu, S.; Liu, H.; Li, J.; Wang, J.; Fan, W. Nanosheet MFI Zeolites for Gas Phase Glycerol Dehydration to Acrolein. *Catalysts* **2019**, *9*, 121. [[CrossRef](#)]
106. Drew, K.; Girishkumar, G.; Vinodgopal, K.; Kamat, P.V. Boosting Fuel Cell Performance with a Semiconductor Photocatalyst: TiO₂/Pt-Ru Hybrid Catalyst for Methanol Oxidation. *Phys. Chem. B Lett.* **2005**, *109*, 11851–11857. [[CrossRef](#)]
107. Parra, R.; Goes, M.S.; Castro, M.S.; Longo, E.; Bueno, P.R.; Varela, J.A. Reaction Pathway to the Synthesis of Anatase via the Chemical Modification of Titanium Isopropoxide with Acetic Acid. *Chem. Mater.* **2008**, *20*, 143–150. [[CrossRef](#)]
108. Long, B.; Zhang, J.; Luo, L.; Ouyang, G.; Balogun, M.S.; Song, S.; Tong, Y. High pseudocapacitance boosts the performance of monolithic porous carbon cloth/closely packed TiO₂ nanodots as an anode of an all-flexible sodium-ion battery. *J. Mater. Chem. A* **2019**, *7*, 2626–2635. [[CrossRef](#)]
109. Babaei, Z.; Chermahini, A.N.; Dinari, M. Glycerol adsorption and mechanism of dehydration to acrolein over TiO₂ surface: A density functional theory study. *J. Colloid Interface Sci.* **2020**, *563*, 1–7. [[CrossRef](#)]
110. Ulgen, A.; Hoelderich, W.F. Conversion of glycerol to acrolein in the presence of WO₃/TiO₂ catalysts. *Appl. Catal. A Gen.* **2011**, *400*, 34–38. [[CrossRef](#)]
111. Wang, X.; Zhao, F.; Huang, L. Low Temperature Dehydration of Glycerol to Acrolein in Vapor Phase with Hydrogen as Dilution: From Catalyst Screening via TPSR to Real-Time Reaction in a Fixed-Bed. *Catalysts* **2020**, *10*, 43. [[CrossRef](#)]
112. Rosas, I.P.; Larios, J.L.C.; Zeifert, B.; Blásquez, J.S. Catalytic Dehydration of Glycerine to Acrolein. In *Glycerine Production and Transformation—An Innovative Platform for Sustainable Biorefinery and Energy*; IntechOpen: London, UK, 2019; pp. 1–19.
113. Basu, S.; Sen, A.K. Dehydration of glycerol with silica–phosphate-supported copper catalyst. *Res. Chem. Intermed.* **2020**, *46*, 3545–3568. [[CrossRef](#)]
114. Basu, S.; Sen, A.K.; Mukherjee, M. Synthesis and performance evaluation of silica-supported copper chromite catalyst for glycerol dehydration to acetol. *J. Chem. Sci.* **2019**, *131*, 82. [[CrossRef](#)]
115. Lima, D.S.; Perez-Lopez, O.W. Preparation of alumina with different precipitants for the gas phase dehydration of glycerol and their characterization by thermal analysis. *J. Therm. Anal. Calorim.* **2020**, *142*, 1387–1398. [[CrossRef](#)]
116. Kim, Y.T.; Jung, K.D.; Park, E.D. Gas-phase dehydration of glycerol over silica–alumina catalysts. *Appl. Catal. B Environ.* **2011**, *107*, 177–187. [[CrossRef](#)]
117. Corma, A.; Huber, G.W.; Sauvanaud, L.; O'Connor, P. Biomass to chemicals: Catalytic conversion of glycerol/water mixtures into acrolein, reaction network. *J. Catal.* **2008**, *257*, 163–171. [[CrossRef](#)]
118. Cavani, F.; Guidetti, S.; Marinelli, L.; Piccinini, M.; Ghedini, E.; Signoretto, M. The control of selectivity in gas-phase glycerol dehydration to acrolein catalysed by sulfated zirconia. *Appl. Catal. B Environ.* **2010**, *100*, 197–204. [[CrossRef](#)]

119. Kim, Y.T.; Jung, K.D.; Park, E.D. Gas-phase dehydration of glycerol over ZSM-5 catalysts. *Microporous Mesoporous Mater.* **2010**, *131*, 28–36. [[CrossRef](#)]
120. De Oliveira, A.S.; Vasconcelos, S.J.S.; de Sousa, J.R.; de Sousa, F.F.; Filho, J.M.; Oliveira, A.C. Catalytic conversion of glycerol to acrolein over modified molecular sieves: Activity and deactivation studies. *Chem. Eng. J.* **2011**, *168*, 765–774. [[CrossRef](#)]
121. Tresatayawed, A.; Glinrun, P.; Jongsomjit, B. Ethanol Dehydration over WO_3/TiO_2 Catalysts Using Titania Derived from Sol-Gel and Solvothermal Methods. *Int. J. Chem. Eng.* **2019**, *2019*, 4936292. [[CrossRef](#)]
122. Dalil, M.; Carnevali, D.; Edeake, M.; Auroux, A.; Dubois, J.L.; Patience, G.S. Gas phase dehydration of glycerol to acrolein: Coke on WO_3/TiO_2 reduces by-products. *J. Mol. Catal. A Chem.* **2016**, *421*, 146–155. [[CrossRef](#)]
123. Akizuki, M.; Sano, K.; Oshima, Y. Effect of supercritical water on the stability of WO_x/TiO_2 and $\text{NbO}_x/\text{TiO}_2$ catalysts during glycerol dehydration. *J. Supercrit. Fluids* **2016**, *113*, 158–165. [[CrossRef](#)]
124. Stošić, D.; Bennici, S.; Couturier, J.L.; Dubois, J.L.; Auroux, A. Influence of surface acid–base properties of zirconia and titania based catalysts on the product selectivity in gas phase dehydration of glycerol. *Catal. Commun.* **2012**, *17*, 23–28. [[CrossRef](#)]
125. Massa, M.; Andersson, A.; Finocchio, E.; Busca, G. Gas-phase dehydration of glycerol to acrolein over Al_2O_3^- , SiO_2^- , and TiO_2^- supported Nb⁻ and W⁻ oxide catalysts. *J. Catal.* **2013**, *307*, 170–184. [[CrossRef](#)]
126. Ding, J.; Ma, T.; Yan, C.; Shao, R.; Xu, W.; Yun, Z. Vapour Phase Dehydration of Glycerol to Acrolein Over Wells–Dawson Type $\text{H}_6\text{P}_2\text{W}_{18}\text{O}_{62}$ Supported on Mesoporous Silica Catalysts Prepared by Supercritical Impregnation. *J. Nanosci. Nanotechnol.* **2018**, *18*, 2463–2471. [[CrossRef](#)] [[PubMed](#)]
127. Cecilia, J.A.; García-Sancho, C.; Mérida-Robles, M.J.; Santamaría-González, J.; Infantes-Molina, A.; Moreno-Tost, R.; Maireles-Torres, P. Aluminum doped mesoporous silica SBA-15 for glycerol dehydration to value-added chemicals. *J. Sol–Gel Sci. Technol.* **2017**, *83*, 342–354. [[CrossRef](#)]
128. Cecilia, J.A.; García-Sancho, C.; Mérida-Robles, J.M.; González-Santamaría, J.; Moreno-Tost, R.; Maireles-Torres, P. WO_3 Supported on Zr Doped Mesoporous SBA-15 Silica for Glycerol Dehydration to Acrolein. *Appl. Catal. A Gen.* **2016**, *516*, 30–40. [[CrossRef](#)]
129. Herbon, M.; Lange, A.; Weiß, M.; Suprun, W.; Enke, D. Silica-Supported Phosphotungstic Acid for Gas Phase Dehydration of Glycerol. *Chem. Eng. Technol.* **2015**, *38*, 431–440. [[CrossRef](#)]
130. Chai, S.H.; Yan, B.; Tao, L.Z.; Liang, Y.; Xu, B.Q. Sustainable production of acrolein: Catalytic gas-phase dehydration of glycerol over dispersed tungsten oxides on alumina, zirconia and silica. *Catal. Today* **2014**, *234*, 215–222. [[CrossRef](#)]
131. Huang, L.; Qin, F.; Huang, Z.; Zhuang, Y.; Ma, J.; Xu, H.; Shen, W. Metal Organic Framework-mediated Synthesis of Small-sized γ -alumina as highly active Catalyst for Dehydration of Glycerol to Acrolein. *ChemCatChem* **2018**, *23*, 381–386. [[CrossRef](#)]
132. Danov, S. Esipovich, A.; Belousov, A.; Rogozhi, A. Gas-Phase Dehydration of Glycerol over Commercial Pt/ γ - Al_2O_3 Catalyst. *Chin. J. Chem. Eng.* **2015**, *23*, 1138–1146. [[CrossRef](#)]
133. Haider, M.H.; Agostino, C.D.; Dummer, N.F.; Mantle, M.D.; Gladden, L.F.; Knight, D.W.; Willock, D.J.; Morgan, D.J.; Taylor, S.H.; Hutchings, G.J. The Effect of Grafting Zirconia and Ceria onto Alumina as a Support for Silicotungstic Acid for the Catalytic Dehydration of Glycerol to Acrolein. *Chem. Eur. J.* **2014**, *3*, 1743–1752. [[CrossRef](#)]
134. Yfanti, V.L.; Lemonidou, A.A. Effect of hydrogen donor on glycerol hydrodeoxygenation to 1,2-propanediol. *Catal. Today* **2019**, *355*, 727–736. [[CrossRef](#)]
135. Milewski, A.; Dydo, P.; Jakóbić-Kolon, A.; Czechowicz, D.; Babilas, D.; Burek, M.; Waśkiewicz, S.; Byczek-Wyrostek, A.; Krawczyk, T.; Kasprzycka, A. Preparation of Triglycerol from Glycerol and Epichlorohydrin at Room Temperature: Synthesis Optimization and Toxicity Studies. *ACS Sustain. Chem. Eng.* **2018**, *6*, 13208–13216. [[CrossRef](#)]
136. Fan, X.; Burton, R.; Zhou, Y. Glycerol (Byproduct of Biodiesel Production) as a Source for Fuels and Chemicals—Mini Review. *Open Fuels Energy Sci. J.* **2010**, *3*, 17–22. [[CrossRef](#)]
137. Sun, D.; Yamada, Y.; Sato, S.; Ueda, W. Glycerol hydrogenolysis into useful C_3 chemicals. *Appl. Catal. B Environ.* **2016**, *193*, 75–92. [[CrossRef](#)]
138. Nakagawa, Y.; Tamura, M.; Tomishige, K. Catalytic materials for the hydrogenolysis of glycerol to 1,3-propanediol. *J. Mater. Chem.* **2014**, *2*, 6688–6702. [[CrossRef](#)]
139. Malleshham, B.; Sudarsanam, P.; Venkat, B.S.R.; Reddy, B.M. Development of Cerium Promoted Copper–Magnesium Catalysts for Biomass Valorization: Selective Hydrogenolysis of Bioglycerol. *Appl. Catal. B Environ.* **2016**, *181*, 47–57. [[CrossRef](#)]
140. Chen, B.; Zhang, D.B.; Zhang, D.Y.; Yang, P.X. Bimetallic Effects of Silver-Modified Nickel Catalysts and their Synergy in Glycerol Hydrogenolysis. *ChemCatChem* **2016**, *8*, 1929–1936. [[CrossRef](#)]
141. Shi, G.; Su, L.; Jin, K. New bulk nickel phosphide catalysts for glycerol hydrogenolysis to 1,2-propanediol. *Catal. Commun.* **2015**, *59*, 180–183. [[CrossRef](#)]
142. Salazar, J.B.; Falcone, D.D.; Pham, H.N.; Datye, A.K.; Passos, F.B.; Davis, R.J. Selective production of 1,2-propanediol by hydrogenolysis of glycerol over bimetallic Ru–Cu nanoparticles supported on TiO_2 . *Appl. Catal. A Gen.* **2014**, *482*, 137–144. [[CrossRef](#)]
143. Liu, L.; Asano, T.; Nakagawa, Y.; Tamura, M.; Okumura, K.; Tomishige, K. Selective Hydrogenolysis of Glycerol to 1,3-Propanediol over Rhenium–Oxide-Modified Iridium Nanoparticles Coating Rutile Titania Support. *ACS Catal.* **2019**, *9*, 10913–10930. [[CrossRef](#)]
144. Skuhrovцова, L.; Kolena, J.; Zdenek, T.; Kocik, J. Cu–Zn–Al mixed oxides as catalysts for the hydrogenolysis of glycerol to 1,2-propanediol. *React. Kinet. Mech. Catal.* **2019**, *127*, 241–257. [[CrossRef](#)]
145. Zhao, H.; Zheng, L.; Li, X.; Chen, P.; Hou, Z. Hydrogenolysis of glycerol to 1,2-propanediol over Cu-based catalysts: A short review. *Catal. Today* **2019**, *107*, 2411–2502. [[CrossRef](#)]

146. Modvig, A.; Kumpidet, C.; Riisager, A.; Albert, J. Ru-Doped Wells–Dawson Polyoxometalate as Efficient Catalyst for Glycerol Hydrogenolysis to propanediols. *Materials* **2019**, *12*, 2175. [[CrossRef](#)] [[PubMed](#)]
147. Raju, N.; Rekha, V.; Abhishek, B.; Kumar, P.M.; Sumana, C.; Lingaiah, N. Studies on continuous selective hydrogenolysis of glycerol over supported Cu-Co bimetallic catalysts. *New J. Chem.* **2020**, *44*, 3122–3128. [[CrossRef](#)]
148. Li, X.; Wu, D. Synthesis of Co-doped micro-mesoporous SAPO-11 zeolite for glycerol hydrogenolysis. *Korean J. Chem. Eng.* **2020**, *37*, 216–223. [[CrossRef](#)]
149. Liang, Y.; Shi, G.; Jin, K. Promotion Effect of Al₂O₃ on Pt–WO_x/SiO₂ Catalysts for Selective Hydrogenolysis of Bioglycerol to 1,3-Propanediol in Liquid Phase. *Catal. Lett.* **2020**, *150*, 2365–2376. [[CrossRef](#)]
150. Li, X.; Xiang, M.; Wu, D. Hydrogenolysis of glycerol over bimetallic Cu–Ni catalysts supported on hierarchically porous SAPO-11 zeolite. *Catal. Commun.* **2019**, *119*, 170–175. [[CrossRef](#)]
151. Xi, Z.; Hong, Z.; Huang, F.; Zhu, Z.; Jia, W.; Li, J. Hydrogenolysis of Glycerol on the ZrO₂-TiO₂ Supported Pt–WO_x Catalyst. *Catalysts* **2020**, *10*, 312. [[CrossRef](#)]
152. Liu, C.; Shang, Y.; Wang, S.; Liu, X.; Wang, X.; Gui, J.; Zhang, C.; Zhu, Y.; Li, Y. Boron oxide modified bifunctional Cu/Al₂O₃ catalysts for the selective hydrogenolysis of glucose to 1,2-propanediol. *Mol. Catal.* **2020**, *485*, 110514. [[CrossRef](#)]
153. Shesterkin, A.A.; Kustov, L.M.; Strekalovaa, A.A.; Kazansky, V.B. Heterogeneous iron-containing nanocatalysts—Promising systems for selective hydrogenation and hydrogenolysis. *Catal. Sci. Technol.* **2020**, *10*, 3160–3174. [[CrossRef](#)]
154. Zhang, B.; Chen, B.; Douthwaite, M.; Tang, L.; Zhang, Y.; Wang, M.; Ma, D. Multiporous Carbon Encapsulated Ni Nanoparticles Promote Glycerol Valorisation towards Hydrogenation against Rearrangement. *Chin. J. Catal.* **2020**, *38*, 439–444.
155. Chimentão, R.J.; Miranda, B.C.; Ruiz, D.; Guiradoc, G.; Medina, F.; Llorca, J.; Santos, J.B.O. Catalytic performance of zinc-supported copper and nickel catalysts in the glycerol hydrogenolysis. *J. Energy Chem.* **2020**, *42*, 185–194. [[CrossRef](#)]
156. Yoda, E.; Ootawa, A. Dehydration of glycerol on H-MFI zeolite investigated by FT-IR. *Appl. Catal. A Gen.* **2009**, *360*, 66–70. [[CrossRef](#)]
157. Coll, D.; Delbecq, F.; Aray, Y.; Sautet, P. Stability of intermediates in the glycerol hydrogenolysis on transition metal catalysts from first principles. *Phys. Chem. Chem. Phys.* **2011**, *13*, 1448–1456. [[CrossRef](#)]
158. Dasari, A.M.; Kiatsimkul, P.; Sutterlin, R.W.; Suppes, J.G. Low-pressure hydrogenolysis of glycerol to propylene glycol. *Appl. Catal. A Gen.* **2005**, *281*, 225. [[CrossRef](#)]
159. Seguel, J.; García, R.; Chimentão, R.J.; García-Fierro, J.L.; Ghampson, I.T.; Escalona, N.; Sepúlveda, C. Thermal Modification Effect on Supported Cu-Based Activated Carbon Catalyst in Hydrogenolysis of Glycerol. *Materials* **2020**, *13*, 603. [[CrossRef](#)]
160. Kumar, P.; Shah, A.K.; Lee, J.H.; Park, Y.H.; Stangar, U.L. Selective hydrogenolysis of glycerol over bifunctional Copper-Magnesium supported catalysts for propanediols synthesis. *Ind. Eng. Chem. Res.* **2020**, *59*, 6506–6516. [[CrossRef](#)]
161. Shan, J.; Liu, H.; Lu, K.; Zhu, S.; Li, J.; Wang, J.; Fan, W. Identification of the dehydration active sites in glycerol hydrogenolysis to 1,2-propanediol over Cu/SiO₂ catalysts. *J. Catal.* **2020**, *383*, 13–23. [[CrossRef](#)]
162. Feng, S.; Zhao, B.; Liang, Y.L.; Liu, L.; Dong, J. Improving Selectivity to 1,3-Propanediol for Glycerol Hydrogenolysis Using W[−] and Al[−] Incorporated SBA-15 as Support for Pt Nanoparticles. *Ind. Eng. Chem. Res.* **2019**, *58*, 2661–2671. [[CrossRef](#)]
163. Niu, Y.; Zhao, B.; Liang, Y.; Liu, L.; Dong, J. Promoting Role of Oxygen Deficiency on a WO₃-Supported Pt Catalyst for Glycerol Hydrogenolysis to 1,3-Propanediol. *Ind. Eng. Chem. Res.* **2020**, *59*, 7389–7397. [[CrossRef](#)]
164. Luo, R.; Zhao, X.; Gong, H.; Qian, W.; Li, D.; Chen, M.; Cui, K.; Wang, J.; Hou, Z. Effect of Tungsten Modification on Zirconium Phosphate-supported Pt Catalyst for Selective Hydrogenolysis of Glycerol to 1-Propanol. *Energy Fuels* **2020**, *34*, 8707–8717. [[CrossRef](#)]
165. Wang, J.; Yang, M.; Wang, A. Selective hydrogenolysis of glycerol to 1,3-propanediol over Pt-W based catalysts. *Chin. J. Catal.* **2020**, *41*, 1311–1319. [[CrossRef](#)]
166. López, A.; Aragón, J.A.; Hernández-Cortez, J.G.; Mosqueira, M.L.; Martínez-Palou, R. Study of hydrotalcite-supported transition metals as catalysts for crude glycerol hydrogenolysis. *Mol. Catal.* **2019**, *468*, 9–18. [[CrossRef](#)]
167. Gandarias, I.; Arias, P.L.; Fernández, S.G.; Requies, J.; Doukkali, M.E.; Güemez, M.B. Hydrogenolysis through catalytic transfer hydrogenation: Glycerol conversion to 1,2-propanediol. *Catal. Today* **2012**, *195*, 22–31. [[CrossRef](#)]
168. Hosgu, H.L.; Yıldız, M.; Gercel, H.F. Hydrogenolysis of Aqueous Glycerol over Raney Nickel Catalyst: Comparison of Pure and Biodiesel By-Product. *Ind. Eng. Chem. Res.* **2012**, *51*, 3863–3869. [[CrossRef](#)]
169. Akiyama, M.; Sato, S.; Takahashi, R.; Inui, K.; Yokota, M. Dehydration–hydrogenation of glycerol into 1,2-propanediol at ambient hydrogen pressure. *Appl. Catal. A Gen.* **2009**, *371*, 60–66. [[CrossRef](#)]
170. Wu, Z.; Mao, Y.; Song, M.; Yin, X.; Zhang, M. Cu/boehmite: A highly active catalyst for hydrogenolysis of glycerol to 1,2-propanediol. *Catal. Commun.* **2013**, *32*, 52–57. [[CrossRef](#)]
171. Zhu, S.; Gao, X.; Zhu, Y.; Zhu, Y.; Zheng, H.; Li, Y. Promoting effect of boron oxide on Cu/SiO₂ catalyst for glycerol hydrogenolysis to 1,2-propanediol. *J. Catal.* **2013**, *303*, 70–79. [[CrossRef](#)]
172. Soares, A.H.; Atia, H.; Armbruster, U.; Passos, F.B.; Martin, A. Platinum, palladium and nickel supported on Fe₃O₄ as catalysts for glycerol aqueous-phase hydrogenolysis and reforming. *Appl. Catal. A Gen.* **2017**, *548*, 179–190. [[CrossRef](#)]
173. Soares, A.V.-H.; Perez, G.; Passos, F.B. Alumina supported bimetallic Pt–Fe catalysts applied to glycerol hydrogenolysis and aqueous phase reforming. *Appl. Catal. A Gen.* **2016**, *185*, 77–87. [[CrossRef](#)]
174. Xia, S.; Du, W.; Zheng, L.; Chen, P.; Hou, Z. A thermally stable and easily recycled core–shell Fe₂O₃@CuMgAl catalyst for hydrogenolysis of glycerol. *Catal. Sci. Technol.* **2014**, *4*, 912–916. [[CrossRef](#)]

175. Jiménez-Morales, I.; Vila, F.; Mariscal, R.; Jiménez-López, A. Hydrogenolysis of glycerol to obtain 1,2-propanediol on Ce-promoted Ni/SBA-15 catalysts. *Appl. Catal. B Environ.* **2012**, *117*, 253–259. [[CrossRef](#)]
176. Menchavez, R.N.; Morra, M.J.; He, B.B. Glycerol Hydrogenolysis using a Ni/Ce-Mg Catalyst for Improved Ethanol and 1,2-Propanediol Selectivities. *Can. J. Chem. Eng.* **2017**, *95*, 1332–1339. [[CrossRef](#)]
177. Jiang, T.; Kong, D.; Xu, K.; Cao, F. Hydrogenolysis of glycerol aqueous solution to glycols over Ni–Co bimetallic catalyst: Effect of ceria promoting. *Appl. Pet. Res.* **2016**, *6*, 135–144. [[CrossRef](#)]
178. Rekha, R.V.; Raju, N.; Sumana, C.; Lingaiah, N. Continuous Hydrogenolysis of Glycerol to 1,2-Propanediol Over Bi-metallic Ni–Ag Supported on γ -Al₂O₃ Catalysts. *Catal. Lett.* **2017**, *147*, 1441–1452. [[CrossRef](#)]
179. Zhou, J.; Zhang, J.; Guo, X.; Mao, J.; Zhang, S. Ag/Al₂O₃ for glycerol hydrogenolysis to 1,2-propanediol: Activity, selectivity and deactivation. *Green Chem.* **2012**, *14*, 156–163. [[CrossRef](#)]
180. Yadav, G.D.; Chandan, P.A.; Tekale, D.P. Hydrogenolysis of Glycerol to 1,2-Propanediol over Nano-Fibrous Ag-OMS-2 Catalysts. *Ind. Eng. Chem. Res.* **2012**, *51*, 1549–1562. [[CrossRef](#)]
181. Oh, J.; Dash, S.; Lee, H. Selective conversion of glycerol to 1,3-propanediol using Pt-sulfated zirconia. *Green Chem.* **2011**, *13*, 2004–2007. [[CrossRef](#)]
182. Qin, L.Z.; Song, M.J.; Chen, C.L. Aqueous-phase deoxygenation of glycerol to 1,3-propanediol over Pt/WO₃/ZrO₂ catalysts in a fixed-bed reactor. *Green Chem.* **2010**, *12*, 1466–1472. [[CrossRef](#)]
183. Jiang, T.; Huai, Q.; Geng, T.; Ying, W.; Xiao, T.; Cao, F. Catalytic performance of Pd–Ni bimetallic catalyst for glycerol hydrogenolysis. *Biomass Bioenerg.* **2015**, *78*, 71–79. [[CrossRef](#)]
184. Isabelle, C.F.; Manfro, R.L.; Souza, M.M.V.M. Hydrogenolysis of glycerol to propylene glycol in continuous system without hydrogen addition over Cu–Ni catalysts. *Appl. Catal. B Environ.* **2018**, *220*, 31–41.
185. Vasiliadou, E.S.; Lemonidou, A.A. Investigating the performance and deactivation behaviour of silica-supported copper catalysts in glycerol hydrogenolysis. *Appl. Catal. A Gen.* **2011**, *396*, 177–185. [[CrossRef](#)]
186. Mane, R.B.; Ghalwadkar, A.A.; Hengne, A.M.; Suryawanshi, Y.R.; Rode, C.V. Role of promoters in copper chromite catalysts for hydrogenolysis of glycerol. *Catal. Today* **2011**, *164*, 447–450. [[CrossRef](#)]